IMMUNOLOGY

MALT1 alternative splicing—A molecular rheostat for balancing immune activation and homeostasis

Thomas J. O'Neill[1]†, Carina Graß[1]†, Andreas Gewies[1]†, Sofia Coelho[1], Torben Gehring[1], Thomas Seeholzer[1], Lesca-Miriam Holdt[2], Andrew Flatley[3], Regina Feederle[3,4,5], Jens Staal[6,7], Rudi Beyaert[6,7], Florian Giesert[8], Wolfgang Wurst[8], Necil Kutukculer[9,10], Ronald Naumann[11], Daniel Krappmann[1,12]*

MALT1 (mucosa-associated lymphoid tissue lymphoma/leukemia protein 1)–TRAF6 [tumor necrosis factor receptor (TNFR)-associated factor 6] interaction drives lymphocyte activation and adaptive immunity, but it also contributes to maintaining immune homeostasis. MALT1 exists in two isoforms that differ only by either encoding two (MALT1A) or one (MALT1B) TRAF6 binding motif (T6BM). The human mutation MALT1 E806D in T6BM2, expressed in both MALT1A and MALT1B, has been associated with an immune disorder combining symptoms of immune deficiency and autoimmunity. Here, we report that the orthologous germline mutation MALT1 E814D is sufficient to induce a fatal autoimmune syndrome in mice. We demonstrate that species-specific differences in the effects of T6BM2 disruptions can be attributed to alterations in MALT1 splicing and that immune homeostasis is restored by genetically enforcing expression of MALT1A in MALT1 E814D mice. Thus, alternative MALT1 splicing allows tuning of TRAF6 association, thereby functioning as a molecular rheostat to balance between optimal immune activation and maintenance of peripheral tolerance.

INTRODUCTION

Antigen engagement on lymphocytes induces formation of the CARD11-BCL10-MALT1 (CBM) signalosome that bridges T or B cell receptor (TCR/BCR) signaling at the immune synapse to downstream effector functions (*1*, *2*). MALT1 (mucosa-associated lymphoid tissue lymphoma/leukemia protein 1) paracaspase (also termed PCASP1) serves a dual role in the CBM complex. As a molecular scaffold, MALT1 recruits the E3 ligase tumor necrosis factor receptor (TNFR)-associated factor 6 (TRAF6) to the CBM complex via two TRAF6 binding motifs (T6BM1/2), thereby fostering canonical nuclear factor κB (NF-κB) signaling (*3*–*6*). In addition, MALT1 acts as a protease, cleaving substrates via its paracaspase domain to modulate immune signaling as well as transcriptional and posttranscriptional responses in lymphocytes (*7*, *8*). MALT1 acts in conventional CD4 and CD8 effector T (T_{conv}) cells to induce an adaptive immune response upon immune activation (*9*–*11*). However, MALT1 is also required for the development and function of immune-suppressive regulatory T (T_{reg}) cells, which are essential for maintenance of peripheral tolerance and prevention of autoimmunity (*9*, *12*–*15*). In mice, targeted mutagenesis of both T6BMs in *Malt1* leads to fatal autoimmune inflammation through uncontrolled MALT1 protease activation and overshooting T_{conv} effector responses (*6*). Thus, the tight balance of MALT1 scaffolding and protease functions in Tconv and T_{reg} cells is critical for immune homeostasis in resting cells, while also allowing for optimal immune reactions to pathogenic antigens.

Two conserved MALT1 splicing isoforms exist, and while the shorter MALT1B contains only the C-terminal T6BM2, MALT1A also contains T6BM1 within the alternatively spliced exon 7 region (*3*). The homozygous missense mutation *MALT1* c.2418G>C, which leads to a conservative substitution of glutamic acid (E) to aspartic acid (D) in MALT1 T6BM2 (MALT1A E806D or MALT1B E795D), has been identified in a patient suffering from a complex immune disorder with symptoms of immunodeficiency and autoimmunity (*16*). While this human missense mutation leads to an E-to-D exchange in T6BM2, the T6BM1 in the alternatively spliced exon 7 is unaffected, suggesting that a hypomorphic mutation in *MALT1B* may be sufficient to cause the immune syndrome (*16*).

Here, we report the occurrence of additional human germline mutations, leading to deletion or disruption of T6BM2 in MALT1. Motivated by these variants, we generated a genetically modified mouse model with the aim to phenocopy the human MALT1 E806D mutation, and to study if disruption of MALT1 T6BM2 is sufficient to cause an immune disorder mimicking the human pathology. The markedly more severe autoimmune inflammation caused by the orthologous MALT1 E814D exchange in mice inspired us to closely investigate how alternative MALT1 splice variants contribute to immune homeostasis and activation. Thereby, we provide evidence that alternative splicing of MALT1 serves as a molecular rheostat that allows for optimal mounting of an adaptive immune response and at the same time prevents overshooting autoimmune reactions.

RESULTS

Human C-terminal *MALT1* mutations cause imbalanced MALT1 scaffolding and protease functions

Malt1 c.2418G>C leading to an E-to-D missense exchange was identified as the first human mutation affecting T6BM2 of MALT1 (*16*). However, the genome aggregation database (gnomAD) lists several

[1]Research Unit Signaling and Translation, Signaling and Immunity, Molecular Targets Therapeutic Center, Helmholtz Zentrum München, Neuherberg, Germany. [2]Institute of Laboratory Medicine, LMU University Hospital, LMU Munich, Munich, Germany. [3]Core Facility Monoclonal Antibodies, Helmholtz Zentrum München, Neuherberg, Germany. [4]German Center for Neurodegenerative Diseases (DZNE), Munich, Germany. [5]Munich Cluster for Systems Neurology (SyNergy), Munich, Germany. [6]Center for Inflammation Research, Unit of Molecular Signal Transduction in Inflammation, VIB, Ghent, Belgium. [7]Department of Biomedical Molecular Biology, Ghent University, Ghent, Belgium. [8]Institute of Stem Cell Research, Helmholtz Zentrum München, Neuherberg, Germany. [9]Department of Pediatric Immunology, Ege University Faculty of Medicine, Izmir, Turkey. [10]Department of Medical Genetics, Ege University Faculty of Medicine, Izmir, Turkey. [11]Max Planck Institute of Molecular Cell Biology and Genetics, Transgenic Core Facility, Dresden, Germany. [12]Faculty of Biology, Ludwig-Maximilians-Universität, Munich, Germany.
*Corresponding author. Email: daniel.krappmann@helmholtz-munich.de
†These authors contributed equally to this work.

heterozygous human germline nonsense, frameshift, missense, or exon 17 splice acceptor site mutations that lead to deletion or mutation of T6BM2 (Fig. 1A) (*17*). Using lentiviral transduction, we reconstituted MALT1 KO NF-κB reporter Jurkat T cells with two nonsense mutations and one frameshift mutation, which all lead to preterminal stops and thus C-terminal truncations. The shortest MALT1 variant terminates at the end of the Ig3 domain, the longest variant just before T6BM2. In either MALT1A or MALT1B, most C-terminal truncations were expressed near-endogenous levels, except for MALT1A H793Pfs*7 and MALT1B H782Pfs*7, in which the short extension by the frameshift most likely caused posttranslational destabilization. While all MALT1B truncations deleting T6BM2 yielded constitutive MALT1 protease activity as evident from cleavage of CYLD and N4BP1 in the absence of stimulation, MALT1A mutants, which can still bind to TRAF6 via T6BM1, remained catalytically inactive in resting cells (Fig. 1B). We analyzed the effects of the human genetic MALT1 variants on NF-κB activation after phorbol 12-myristate 13-acetate (PMA)/ionomycin (P/I) or CD3/CD28 stimulation (Fig. 1, C and D). Despite MALT1A H793Pfs*9 that was expressed at lower level, the truncating mutations in MALT1A were fully functional and TCR-induced NF-κB activation was not significantly decreased in comparison to MALT1A wild type (WT). However, NF-κB activation was severely impaired in Jurkat T cells expressing MALT1B truncations. Therefore, within the human population, deletion or defective T6BM2 mutations exist that do not affect downstream functions of MALT1A, but the same mutations abolish inducible scaffolding and enhance constitutive protease functions of MALT1B. Thus, the data suggest that the tight control of MALT1A and MALT1B alternative splicing may govern the balance between immune activation versus homeostasis.

Destruction of T6BM2 in *Malt1*$^{ED/ED}$ mice causes fatal autoimmune inflammation

GnomAD lists four heterozygous missense variants at MALT1A E806Q/G or MALT1B E795Q/G, yielding a potentially destructive missense mutation in the T6BM2 of MALT1 (Fig. 1A). The previously identified MALT1 E806D variant in the homozygous patient and heterozygous parents represents the most conservative alteration at this position (*16*). To assess the impact of the mutation on TRAF6 binding, we quantitatively compared affinities of TRAF6 to MALT1 T6BM2 WT or mutant (E806D and E806A) as well as to the T6BM1 WT (fig. S1). Dose titration revealed similar dissociation constants (K_d) of ~7 and ~10 nM for the binding of the TRAF domain of TRAF6 (amino acids 310 to 522) to WT MALT1 T6BM1 and T6BM2 peptides, respectively. Either E/A or E/D exchange in T6BM2 completely abrogated binding to TRAF6, showing that the patient-derived

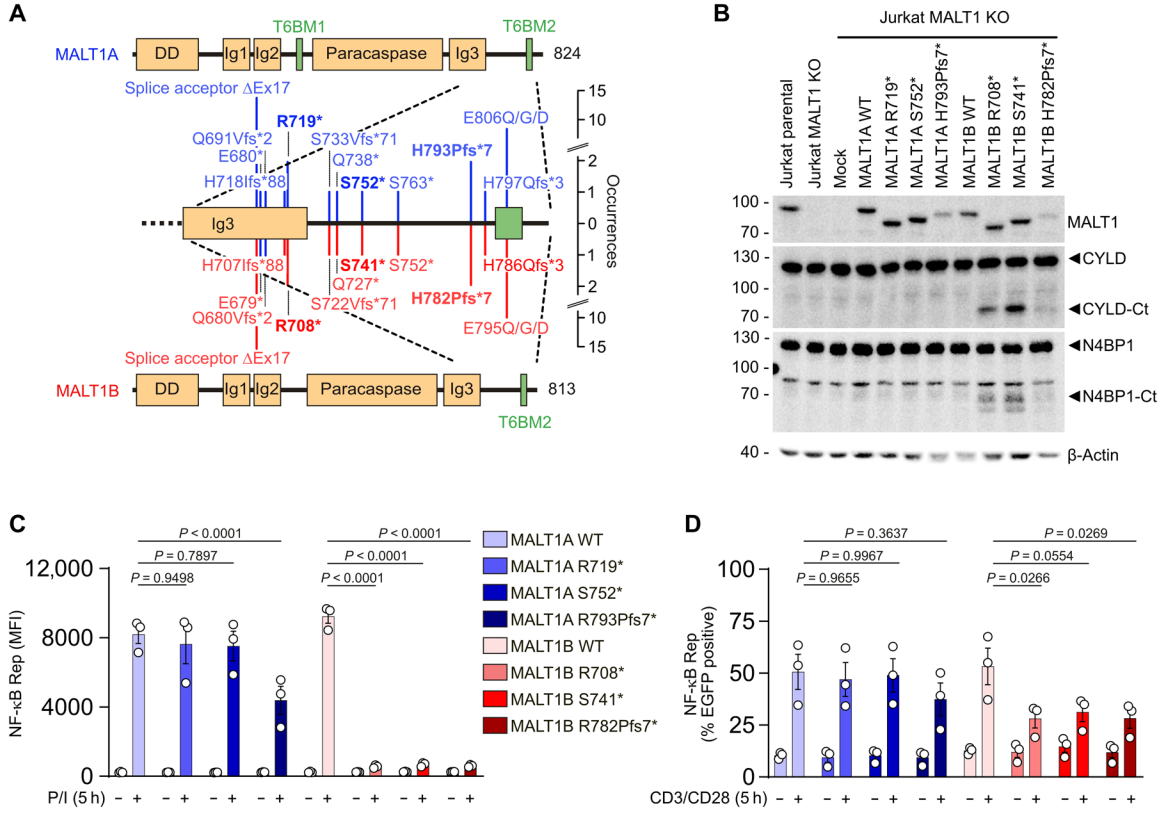

Fig. 1. Homologous patient-derived MALT1 T6BM2 mutations induce constitutive MALT1 activity in vitro and fatal autoimmune inflammation in mice. (**A**) Scheme of heterozygous mutations found in the GNOMAD human genome database yielding point mutations or C-terminal truncations affecting the MALT1B-TRAF6 interaction. Mutations marked in bold were cloned in MALT1A and MALT1B and expressed homozygously in MALT1 knockout Jurkat T cells. (**B**) Analysis of constitutive MALT1 substrate cleavage in unstimulated Jurkat T cell lysates by Western blot. (**C** and **D**) NF-κB reporter analysis of Jurkat T cells by flow cytometry following 5-hour stimulation with P/I (C) or CD3/CD28 (D). Analyses in (C) and (D) were run in triplicate, and values in (C) represent raw MFI values. All bars show the mean ± SEM and *P* values were calculated by two-way analysis of variance (ANOVA) combined with Šidák's multiple comparisons test.

MALT1 c.2418G>C transversion leads to a complete loss of function with respect to MALT1B-TRAF6 interaction, in line with the critical role for T6BM2 in binding of MALT1B to TRAF6 (*3*, *16*).

We wanted to generate a mouse model that recapitulates the in vivo effects of selective destruction of the T6BM2, leading to loss of TRAF6 binding to MALT1B, but not MALT1A, where a functional T6BM1 is still present. We decided to mirror the human *MALT1* c.2418G>C transversion in mice by introducing mutations at the orthologous position in exon 17 of murine *Malt1* (c.2442G>C) using CRISPR-Cas9 and homology-directed repair (HDR) in zygotes of C57BL/6N mice (fig. S2A). In the murine MALT1 protein, this corresponds to the missense mutation at E814D in MALT1A and E803D in MALT1B, respectively (Fig. 2A), henceforth referred to as *Malt1* ED mice. Founders were backcrossed with C57BL/6N WT mice to obtain heterozygous *Malt1*$^{ED/+}$ mice, which were further intercrossed to generate homozygous *Malt1*$^{ED/ED}$ mice. Correct mutations, including silent mutations to prevent continued CRISPR guide recognition after HDR, were verified by genomic PCR genotyping using nested primers and sequencing (fig. S2, B to D).

Homozygous *Malt1*$^{ED/ED}$ mice were born at approximately Mendelian ratio and developed normally until the age of 12 to 14 days, beyond which mice stopped gaining weight and thriving, necessitating euthanasia at a median age of 17 days (Fig. 2, B and C). To determine the phenotypic changes triggering early lethality, all subsequent analyses were performed using mice at 12 to 14 days of age before onset of burden. Heterozygous *Malt1*$^{ED/+}$ mice did not display any signs of an immune phenotype when compared to *Malt1*$^{+/+}$ control mice. However, homozygous *Malt1*$^{ED/ED}$ mice developed lymphadenopathy and splenomegaly (Fig. 2D and fig. S2E). Relative numbers of splenic CD3$^+$ T and B220$^+$ B cells were reduced in *Malt1*$^{ED/ED}$ mice (Fig. 2E), but T and B lymphocytes were highly activated in spleen and lymph nodes as revealed by elevated CD44^{hi}CD62L^{lo} effector memory-like T (T_{EM}) cells and high proportions of CD69$^+$ T and B cells and CD86$^+$ B cells (Fig. 2, F to H, and fig. S2, F to H). Numbers of suppressive splenic CD4$^+$FoxP3$^+$ T_{reg} cells were within the normal range in spleen, but significantly elevated in lymph nodes (Fig. 2I and fig. S2I). The fraction of effector T_{reg} cells (eTregs: CD4$^+$CD44^{hi}CD62L^{lo}) was increased in the spleen, with expression of the functional markers Ox40, CTLA-4, and PD-1 on eT_{reg} cells being equal or elevated in *Malt1*$^{ED/ED}$ mice compared with controls, indicating that T_{reg} cells are present and functional (fig. S2, J and K). Increased activation of T_{conv} cells coincided with elevated concentrations of

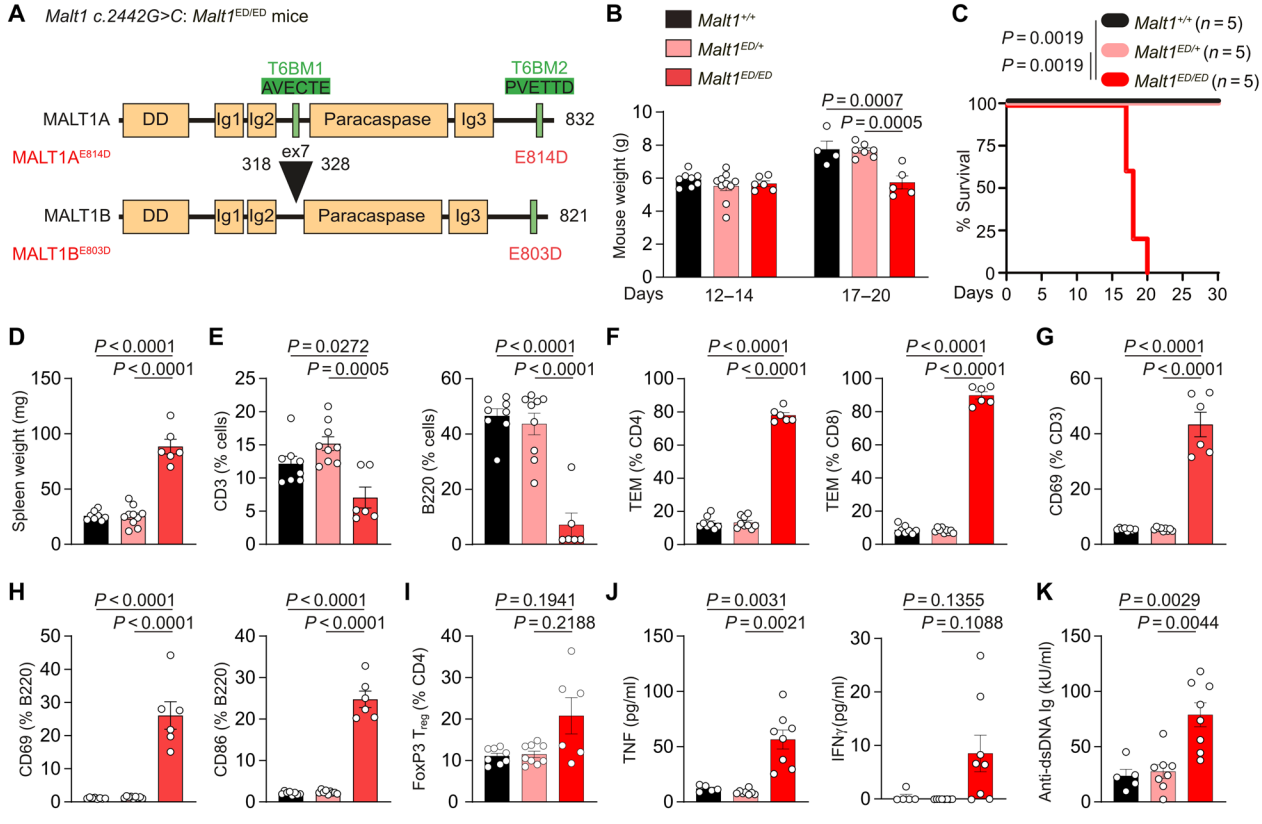

Fig. 2. Homologous patient-derived MALT1 ED mutation in T6BM2 causes fatal autoimmune inflammation in C57BL6/N mice. (**A**) Scheme of Glu to Asp [(E) to (D)] exchange in TRAF6 binding motif 2 (T6BM2) of MALT1A and MALT1B. (**B**) Mouse weights of *Malt1*$^{+/+}$, *Malt1*$^{ED/+}$, and *Malt1*$^{ED/ED}$ at the ages of 12 to 14 and 17 to 20 days. (**C**) Survival curves of *Malt1*$^{ED/ED}$ and control mice. Statistics for survival were calculated using a log-rank test. (**D**) Spleen weights of *Malt1*$^{ED/ED}$ and control mice. (**E**) Relative percentages of CD3$^+$ and B220$^+$ lymphocytes in spleen of *Malt1*$^{ED/ED}$ and control mice. (**F**) Relative numbers of CD4$^+$ and CD8$^+$CD44^{hi}CD62L^{lo} effector memory T (T_{EM}) cells from spleen. (**G** and **H**) Relative percentages of CD3$^+$CD69$^+$ and B220$^+$CD69$^+$ (G) and B220$^+$ CD86$^+$ (H) cells from spleen. (**I**) Relative numbers of CD4$^+$FoxP3$^+$ regulatory T (T_{reg}) cells from spleen. (**J** and **K**) Concentrations of TNFα and IFN-γ (J) and anti-dsDNA immunoglobulin (K) in the sera. Analyses in (D) to (K) were performed with animals on days 12 to 14 after birth and *Malt1*$^{ED/ED}$ (red) mice were compared to *Malt1*$^{+/+}$ (black) and heterozygous *Malt1*$^{ED/+}$ (pink) littermates. $N = 4$ to 10 for each group. Each dot represents one mouse. All bars show the mean ± SEM and *P* values were calculated by two-way ANOVA combined with Tukey's multiple comparisons test (B) or Welch's one-way ANOVA followed by Games-Howell multiple comparisons test [(D) to (K)].

the cytokines tumor necrosis factor (TNF) and interferon-γ (IFN-γ) and an increase in anti–double-stranded DNA (dsDNA) autoantibodies in sera of *Malt1*$^{ED/ED}$ mice (Fig. 2, J and K). Thus, mice carrying the homozygous E/D exchange in MALT1 T6BM2 suffer from autoimmune inflammation similar to *Malt1* TRAF6 binding mutant (TBM) mice, in which both functional T6BMs are defective (*6*). Clearly, the manifestation of the immune pathology is much more severe than in the human patient expressing the homozygous MALT1 E806D variant (*16*).

Early anemia and liver damage in *Malt1*$^{ED/ED}$ mice

Twelve to fourteen days after birth, bones of *Malt1*$^{ED/ED}$ appeared transparent and fragile compared to *Malt1*$^{ED/+}$ mice as exemplified for tibia and femur (Fig. 3A). To explore whether this correlates with the development of anemia, we performed whole blood cell counts and analyzed essential clinical hematologic and chemical parameters at 12 to 14 days of age. In *Malt1*$^{+/+}$ and *Malt1*$^{ED/+}$ control mice, blood cell counts were within the expected range for ~2-week-old C57BL/6 mice (*18*). In *Malt1*$^{ED/ED}$ mice, average leukocyte numbers were spread but not significantly increased, while erythrocyte counts severely dropped (Fig. 3, B and C). In line with this, hemoglobin and hematocrit levels were significantly reduced in *Malt1*$^{ED/ED}$, consistent with a reduced oxygen-carrying capacity and the development of early-onset anemia as a first disease marker (Fig. 3, D and E). In addition, we measured clinical parameters in the serum as indicators of potential organ damage. While alanine aminotransferase (ALT), lactate dehydrogenase (LDH), and aspartate aminotransferase (AST) were not significantly increased when looking at all mice, the concentration of glutamate dehydrogenase (GLDH) was significantly higher in *Malt1*$^{ED/ED}$ mice (Fig. 3, F to I). Closer inspection showed that the two mice (blue dots) with the smallest number of erythrocytes and lowest hemoglobin and hematocrit displayed severely increased values in all four clinical parameters indicative of liver injury. Thus, in-depth phenotypic analyses of homozygous *Malt1*$^{ED/ED}$ mice on days 12 to 14 after birth captures the early-onset autoimmune inflammation, which causes rapidly progressing anemia, eventually leading to secondary damage of the liver and most likely other tissues, requiring euthanasia 2 to 3 weeks after birth.

Defective NF-κB and chronic MALT1 protease activation in *Malt1*$^{ED/ED}$ lymphocytes

The patient with the *MALT1* c.2418G>C transversion and the corresponding homozygous MALT1 E806D substitution has been diagnosed with chronic otitis and recurrent bronchial infections, indicating compromised immune responses (*16*). We therefore analyzed immune signaling in splenocytes isolated from *Malt1*$^{+/+}$, *Malt1*$^{ED/+}$, and *Malt1*$^{ED/ED}$ mice after stimulation with P/I or anti-CD3/CD28. Biochemical analyses in total splenocytes showed impaired IκBα degradation and p65 phosphorylation after P/I stimulation in *Malt1*$^{ED/ED}$ compared to *Malt1*$^{+/+}$ or *Malt1*$^{ED/+}$ mice (Fig. 4A). To quantify NF-κB signaling in T and B cells on the single-cell level, we determined IκBα protein amounts gated on CD4$^+$ T or CD19$^+$ B lymphocytes before and after stimulation by flow cytometry (Fig. 4, B to D). Steady-state IκBα levels were consistently higher in T and B cells from *Malt1*$^{ED/ED}$ mice compared with either *Malt1*$^{+/+}$ or *Malt1*$^{ED/+}$ mice (Fig. 4B). While antigenic stimulation induced a similar degradation of IκBα in T and B cells of *Malt1*$^{+/+}$ and *Malt1*$^{ED/+}$ control mice, IκBα was not degraded in lymphocytes from *Malt1*$^{ED/ED}$ mice (Fig. 4, C and D). Splenocytes from *Malt1*$^{ED/ED}$ mice showed cleavage of the various MALT1 substrates such as N4BP1, CYLD, Regnase-1, and HOIL-1 in the absence of stimulation, indicating chronic MALT1 paracaspase activity (Fig. 4E). To determine the functional effects of chronic MALT1 protease activity, we analyzed protein expression of the Roquin-1/2 and Regnase-1 posttranscriptional target mRNAs NFKBID/IκBNS and inducible T cell costimulator (ICOS) (*6*, *19*, *20*). Both IκBNS and ICOS were up-regulated in CD4$^+$ and CD8$^+$ T cells

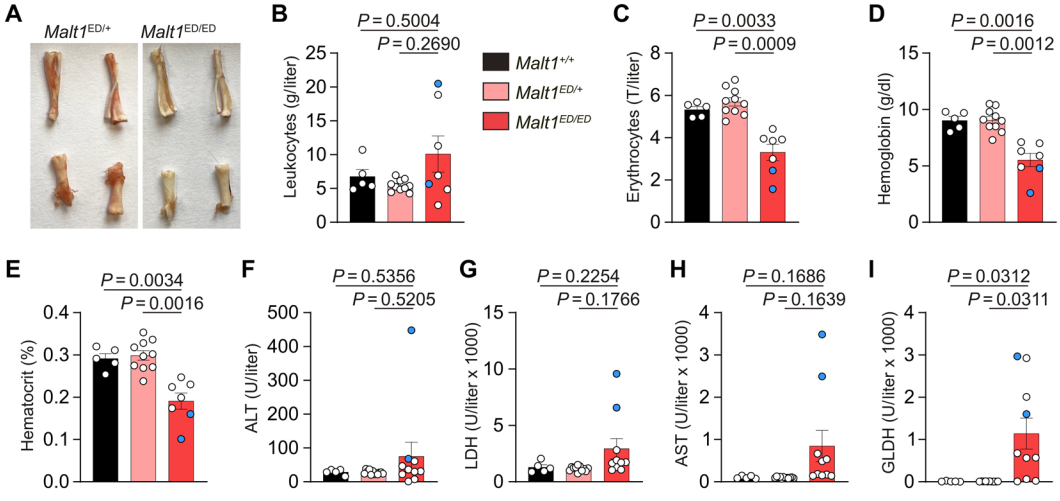

Fig. 3. Early lethality of *Malt1* ED mice is caused by anemia and concomitant liver damage. (**A**) Representative pictures of femur bones of *Malt1*$^{ED/+}$ and *Malt1*$^{ED/ED}$ mice. (**B** to **E**) Hematological parameters of *Malt1*$^{+/+}$, *Malt1*$^{ED/+}$, and *Malt1*$^{ED/ED}$ mice. Leukocytes (B), erythrocytes (C), hemoglobin (D), and hematocrit (E) concentrations are shown. (**F** to **I**) Clinical chemistry parameters. Alanine aminotransferase [ALT; (F)], lactate dehydrogenase [LDH; (G)], aspartate aminotransferase [AST; (H)], and glutamate dehydrogenase [GLDH; (I)] are shown. Analyses were performed with animals on days 12 to 14 after birth and *Malt1*$^{ED/ED}$ (red) mice were compared to *Malt1*$^{+/+}$ (black) and heterozygous *Malt1*$^{ED/+}$ (pink) littermates. $N = 5$ to 12 for each group. Each dot represents one mouse and the two individual mice with lowest blood counts and highest clinical parameters are depicted in blue. All bars show the mean ± SEM and *P* values were calculated by Welch's one-way ANOVA followed by Games-Howell multiple comparisons test [(B) to (I)].

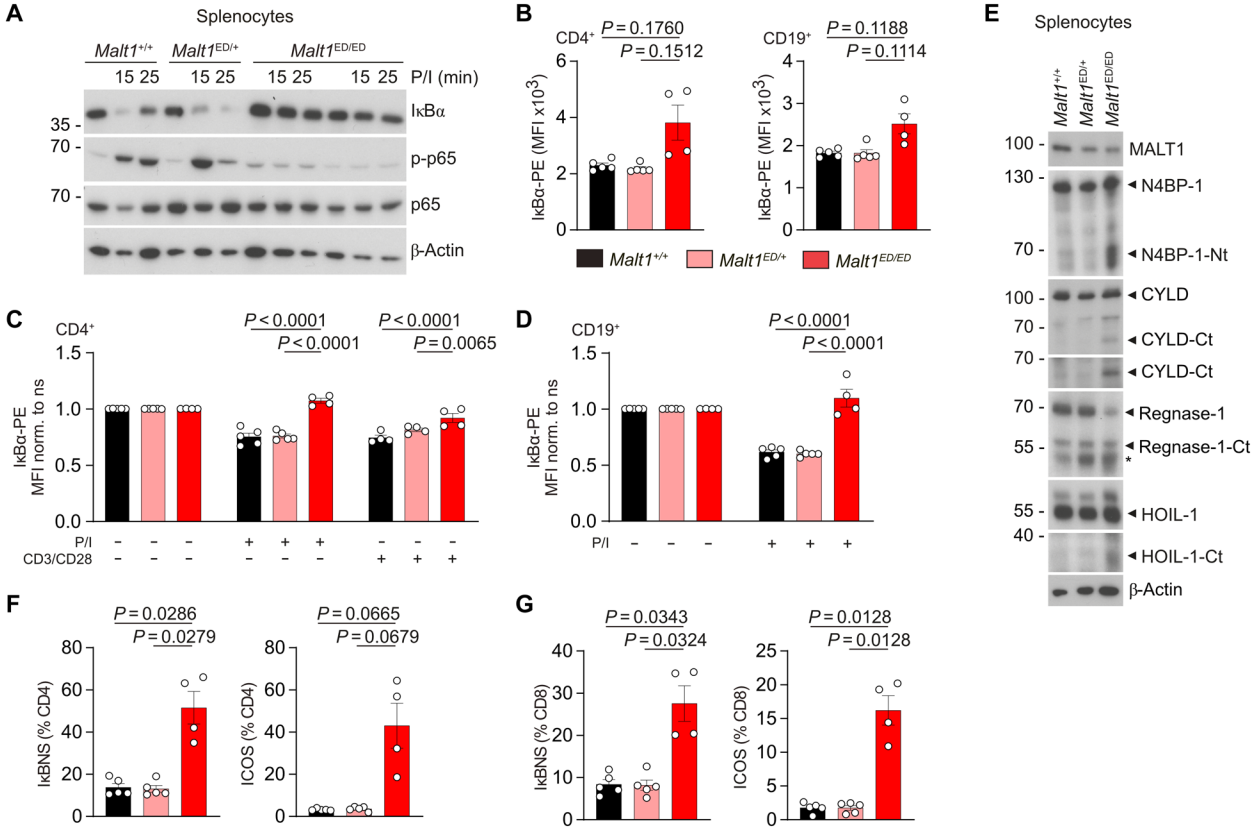

Fig. 4. MALT1 ED mutation causes defective NF-κB signaling and chronic MALT1 protease activation. (**A**) WB analysis of P/I-inducible canonical NF-κB signaling (IκBα degradation and p-p65) in splenocytes *Malt1*$^{+/+}$, *Malt1*$^{ED/+}$, and *Malt1*$^{ED/ED}$ mice. (**B**) Flow cytometry analysis of IκBα protein amounts in unstimulated CD4$^+$ T and CD19$^+$ B cells. (**C** and **D**) Flow cytometry analysis of IκBα degradation in PMA/ionomycin (P/I) or anti-CD3/CD28 stimulated CD4$^+$ (C) or P/I stimulated CD19$^+$ (D) lymphocytes of *Malt1*$^{+/+}$, *Malt1*$^{ED/+}$, and *Malt1*$^{ED/ED}$ mice. Mean fluorescence intensity (MFI) is normalized to unstimulated cells. (**E**) WB analysis of constitutive MALT1 substrate cleavage in splenocytes from *Malt1*$^{+/+}$, *Malt1*$^{ED/+}$, and *Malt1*$^{ED/ED}$ mice. Asterisk indicates unspecific signal. (**F** and **G**) Expression of ICOS and IκBNS in CD4$^+$ (F) and CD8$^+$ (G) T cells by flow cytometric analysis of spleen of *Malt1*$^{+/+}$, *Malt1*$^{ED/+}$, and *Malt1*$^{ED/ED}$ mice. All analyses were performed with animals on days 12 to 14 after birth and *Malt1*$^{ED/ED}$ (red) mice were compared to *Malt1*$^{+/+}$ (black) and heterozygous *Malt1*$^{ED/+}$ (pink) littermates. $N = 4$ to 5 for each group. Each dot represents one mouse. All bars show the mean ± SEM and P values were calculated by two-way ANOVA combined with Tukey's multiple comparisons test [(C) and (D)] or Welch's one-way ANOVA followed by Games-Howell multiple comparisons test [(B), (F), and (G)].

from *Malt1*$^{ED/ED}$ mice (Fig. 4, F and G). Thus, selective destruction of T6BM2 by a conservative E814D exchange is sufficient to cause defective antigen-induced canonical NF-κB activation in lymphocytes, while at the same time inducing chronic MALT1 protease activity, implying that the regulation of MALT1 functions by TRAF6 controls and balances T cell activation in *Malt1* ED mice.

Differences in MALT1 alternative splicing in human and murine immune cells

Phenotypic alterations of *Malt1*$^{ED/ED}$ mice resemble the fatal autoimmune phenotype of homozygous *Malt1* TBM mice, in which both T6BM1 and T6BM2 have been mutated (*6*). However, in humans, the homologous T6BM2 mutation causes a complex but less severe immune disorder with characteristics of combined immune deficiency and autoimmunity (*16*). We determined whether differential expression of the MALT1 splice isoforms might be responsible for the observed discrepancies in immune pathology. We compared relative *MALT1A*/*MALT1B* mRNA expression using the vertebrate alternative splicing and transcription database (VastDB), an atlas of alternative splicing profiles across multiple vertebrate tissues and cells (*21*). While *MALT1A* is the most abundant isoform in most human tissues, *Malt1B* is the major isoform in murine organs (Fig. 5A). However, in the hematopoietic organs thymus, lymph nodes, and spleen *MALT1B* by far exceed *MALT1A* transcripts. With few exceptions, *MALT1B* is the major isoform in most immune tissues (spleen, thymus, and lymph nodes) and cells (macrophages and white blood cells) of mammals depicted in the VastDB database, while *MALT1A* is the major isoform in the skin (fig. S3A). Of note, *Malt1A* transcripts are virtually absent in any immune tissues and cells of mice, but also in the skin and other nonhematopoietic tissues, the *Malt1A*/*Malt1B* ratio is between ~1/3 (colon and liver) and ~1/25 (heart), revealing that *Malt1B* is the major splice variant in mice (Fig. 5A and fig. S3A). In contrast, low *MALT1A* transcripts (~5 to 20% of total *MALT1*) are detected in human lymph nodes, spleen, and white blood cells. In line with this, qualitative and quantitative reverse transcription polymerase chain reaction (RT-PCR) analysis demonstrated that both *Malt1A* and *Malt1B* are expressed in liver, lung, and skin, but *Malt1A* is barely or is not detectable in spleen, lymph nodes, thymus, or lymphocytes of C57BL/6N mice (Fig. 5, B and C, and fig. S3B). Direct comparison revealed that low *MALT1A* expression is detectable

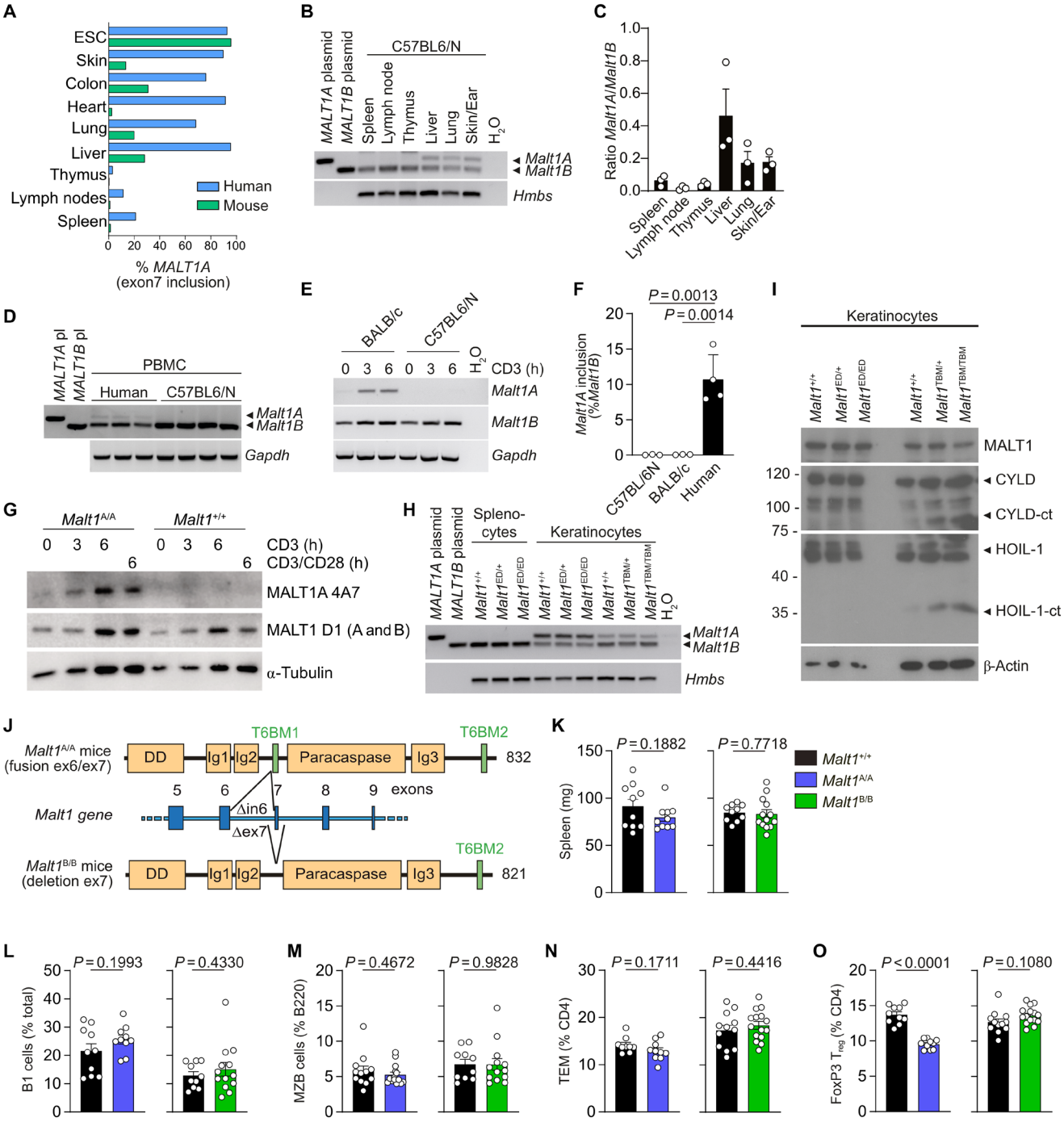

Fig. 5. Differential MALT1 isoform expression and phenotype of MALT1 isoform-specific mice. (**A**) *MALT1A* expression in human and murine tissues according to the VastDB database. (**B**) RT-PCR analysis of *Malt1A/B* expression in murine tissue with *Hmbs* as control. (**C**) Relative *Malt1A/B* mRNA expression in murine tissue analyzed by qRT-PCR. (**D**) RT-PCR analysis of *MALT1A/B* mRNA expression in human and murine PBMCs. (**E**) Isoform-specific RT-PCR analysis of *Malt1A/B* mRNA expression in $CD4^+$ T cells from spleen of BALB/c and C57BL6/N mice upon stimulation with *Gapdh* as control. (**F**) Transcript ratio of *Malt1A* and *B* isoforms in $CD4^+$ T cells from spleen or blood of mice and humans, respectively. (**G**) MALT1 protein expression using MALT1A-specific (4A7/R2C) or total MALT1 (D1) antibodies in $CD4^+$ T cells from $Malt1^{+/+}$ and $Malt1^{A/A}$ mice upon stimulation. (**H**) RT-PCR analysis of *Malt1A/B* mRNA expression in splenocytes and keratinocytes from $Malt1^{TBM/TBM}$ and $Malt1^{ED/ED}$ mice and littermate controls with *Hmbs* as control. (**I**) Analysis of CYLD and HOIL-1 cleavage in keratinocytes from $Malt1^{TBM/TBM}$ and $Malt1^{ED/ED}$ mice and littermate controls. (**J**) Scheme of genomic alterations to generate exon 6/7 fusion for exclusive expression of *Malt1* isoform A ($Malt1^{A/A}$ mice) and genomic exon 7 deletion for exclusive expression of *Malt1* isoform B ($Malt1^{B/B}$ mice). (**K**) Spleen weights of $Malt1^{A/A}$ (blue) and $Malt1^{B/B}$ (green) and littermate controls (black). (**L** to **O**) Immunophenotyping of 10- to 12-week-old $Malt1^{A/A}$, $Malt1^{B/B}$, and $Malt1^{+/+}$ mice: Relative numbers of B1 cells from peritoneal cavity (L), splenic marginal zone (MZ) B cells (M), splenic $CD4^+CD44^{hi}CD62L^{lo}$ effector memory T (T_{EM}) cells (N), and splenic $CD4^+FoxP3^+$ T_{reg} cells (O). $N = 3$ to 4 [(C) and (F)] and 10 to 15 [(K) to (O)] for each group. Each dot represents one mouse. All bars show mean ± SEM and *P* values via unpaired *t* test with Welch's correction [(K) to (O)] or via one-way ANOVA combined with Tukey's multiple comparisons test (F).

in human but not in murine peripheral blood mononuclear cells (PBMCs) (Fig. 5D). We compared *Malt1A* and *Malt1B* transcripts in $CD4^+$ T cells from various mouse strains (C57BL/6N, CD-1, 129S2/Sv, and BALB/c) (Fig. 5E and fig. S3C). All strains display very low levels of *Malt1A* in $CD4^+$ T cells, and *Malt1A* expression could be induced by CD3 or CD3/CD28 stimulation, but inducible *Malt1A* expression was not seen in T cells of C57BL/6N mice. By quantifying absolute transcript numbers in $CD4^+$ T cells from BALB/c and C57BL/6N mice and human donors, we show that there were hardly any *Malt1A* transcripts detectable in mice (<0.1%), whereas human *MALT1* transcripts are approximately 10% *MALT1A* (Fig. 5F and fig. S3, D and E).

To confirm lack of MALT1A expression on protein level in mice, we generated a monoclonal antibody that selectively recognizes exon 7, which is selectively included in MALT1A with identical protein sequence in human and mouse (*3*). Anti-MALT1A 4A7 antibody detects only MALT1A but not MALT1B transduced into MALT1 KO Jurkat T cells in Western blot or flow cytometry (fig. S3, F and G). Mild endogenous expression of MALT1A is also detected in human Jurkat T cells. However, anti-MALT1A 4A7 was unable to detect any MALT1A protein in lymphocytes or monocytes from C57BL/6N mice by either flow cytometry or Western blotting, but detected MALT1A in $Malt1^{A/A}$ or $Malt1^{A/+}$ mice, which we engineered to force exon 7 inclusion and thus enable MALT1A expression in mice ($Malt1^{A/A}$, described in more detail below) (Fig. 5G and fig. S3H). Thus, MALT1B but not MALT1A is expressed in murine immune cells, while some MALT1A expression is retained in human lymphocytes.

Expression of MALT1A can counteract constitutive MALT1 protease caused by destruction of T6BM2

While murine splenocytes are devoid of *Malt1*A, considerable amounts are expressed in murine skin (Fig. 5, A to C, and fig. S3A). Thus, we chose keratinocytes as a cellular model system to study the impact of a functional T6BM1 in MALT1A for counteracting constitutive MALT1 protease activation caused by a defective T6BM2 in MALT1B. To this end, we isolated keratinocytes from $Malt1^{+/+}$, $Malt1^{ED/ED}$ (defective T6BM2), and $Malt1^{TBM/TBM}$ (defective T6BM1 and 2) mice and respective heterozygous littermate controls (*6*). We confirmed that keratinocytes of these mouse strains express substantial amounts of *Malt1*A and *Malt1B*, whereas splenocyte exclusively express *Malt1B* (Fig. 5H). We tested for constitutive cleavage of MALT1 substrates CYLD and HOIL-1 in keratinocytes. While destruction of the C-terminal T6BM2 in keratinocytes of $Malt1^{ED/ED}$ or $Malt1^{ED/+}$ mice did not trigger constitutive MALT1 protease activation, destruction of both T6BMs in $Malt1^{TBM/TBM}$ and, to a lesser extent, of one allele in heterozygous $Malt1^{TBM/+}$ keratinocytes resulted in constitutive cleavage of MALT1 substrates (Fig. 5I). Thus, analyses of keratinocytes that express both MALT1 isoforms reveal that an intact T6BM1 in MALT1A counteracts constitutive protease activity caused by the destruction of T6BM2 in MALT1B.

Normal immune homeostasis and activation in mice expressing only MALT1A or MALT1B

To address the biological relevance for the existence of alternative MALT1 splice isoforms, we produced two mouse lines with exclusive expression of either MALT1A ($Malt1^{A/A}$ mice) or MALT1B ($Malt1^{B/B}$ mice) using CRISPR-Cas9 gene editing. $Malt1^{A/A}$ mice were generated by full deletion of intron 6 coupled with an HDR template that directs an in-frame fusion of exon 6 and exon 7, thereby preventing exon 7 skipping and forcing MALT1A expression (Fig. 5J and fig. S4A). $Malt1^{B/B}$ mice were generated by nonhomologous end-joining using sgRNAs flanking exon 7, leading to abolishment of MALT1A expression by permanent exclusion of exon 7 (Fig. 5J and fig. S4B). Successful genetic alterations were verified in the MALT1A and MALT1B mouse lines by genomic PCR and sequencing (fig. S4, A and B). PCR confirmed exclusive *Malt1A* and *Malt1B* expression in the respective mouse strains, as well as undetectable levels of *Malt1A* in C57BL/6N mice (fig. S4C). Total MALT1 protein was expressed at regular levels in splenocytes of $Malt1^{+/+}$, $Malt1^{A/A}$, and $Malt1^{B/B}$ mice, confirming that the genetic alterations did not disrupt MALT1 expression (fig. S4, D and E). MALT1A protein expression was verified on protein level in $Malt1^{A/A}$ or $Malt1^{A/+}$ mice using the anti-MALT1A 4A7 antibody (see Fig. 5G and fig. S3H).

$Malt1^{A/A}$ and $Malt1^{B/B}$ mice were born at Mendelian ratios and were viable and fertile. We monitored body weight until 20 weeks of age, and $Malt1^{A/A}$ and $Malt1^{B/B}$ mice did not show significant differences in weight gain compared to WT controls (fig. S5, A and B). No macroscopic phenotypic alterations were observed up to the age of 12 months. Immune monitoring at 16 weeks of age did not reveal significant differences in spleen weight or relative numbers of lymphocytes populations ($B220^+$, $CD3^+$, $CD4^+$, and $CD8^+$ cells) in the spleen (Fig. 5K and fig. S5, C to F). Biochemical analyses revealed no qualitative differences in NF-κB signaling and MALT1 protease activation in splenocytes of $Malt1^{A/A}$ and $Malt1^{B/B}$ mice (fig. S5, G and H). $CD4^+$ T cells did not show differences in proliferative responses upon anti-CD3/CD28 stimulation (fig. S5I). We focused on analyzing lymphocyte populations that are known to be affected in mice with *Malt1* knockout ($Malt1^{-/-}$), protease-deficiency ($Malt1^{PD/PD}$), or TRAF6 binding mutation ($Malt1^{TBM/TBM}$). B1 cell and marginal zone (MZ) B cell populations, which are strongly diminished in $Malt1^{-/-}$ or $Malt1^{PD/PD}$ mice, are normal in $Malt1^{A/A}$ and $Malt1^{B/B}$ mice (Fig. 5, L and M) (*10*–*14*). Further, frequencies of $CD4^+$ T_{EM} cells, which are massively expanded in $Malt1^{TBM/TBM}$ and $Malt1^{ED/ED}$ mice, were unchanged in both isoform-specific mice (Fig. 5N). However, while thymic T_{reg} cells were not reduced, young and aged $Malt1^{A/A}$ but not $Malt1^{B/B}$ mice displayed a moderate but consistent reduction in frequencies of peripheral T_{reg} cells (Fig. 5O and fig. S5, J and K). We immunized $Malt1^{A/A}$ and $Malt1^{B/B}$ mice with NP-Ova, but we did not observe changes in T cell–dependent IgG1 production in the serum (fig. S5, L and M). Thus, even though alternative splicing of *Malt1* is tightly regulated and MALT1B is the major isoform in mice, forced exclusive expression of either MALT1A or MALT1B does not cause major immunophenotypic alterations under homeostatic or activated conditions, besides a mild reduction in peripheral T_{reg} cells in the absence of MALT1B.

MALT1A expression rescues autoimmune inflammation caused by T6BM2 destruction

To test whether MALT1A expression in human immune cells may be responsible for milder disease progression in the human patient with a destructive E806D mutation in T6BM2—compared to the acute early-onset disease in $Malt1^{ED/ED}$ mice—we determined whether the inflammatory phenotype of $Malt1^{ED/ED}$ mice can be ameliorated by enforced MALT1A expression. To this end, we introduced the *Malt1* E814D mutation into zygotes of $Malt1^{A/A}$ mice using CRISPR-Cas9 with HDR, resulting in mice carrying the orthologous patient-derived T6BM2 mutation in the context of mice exclusively expressing MALT1A ($Malt1^{A\text{-}ED/A\text{-}ED}$ mice) (Fig. 6A). In contrast to $Malt1^{ED/ED}$

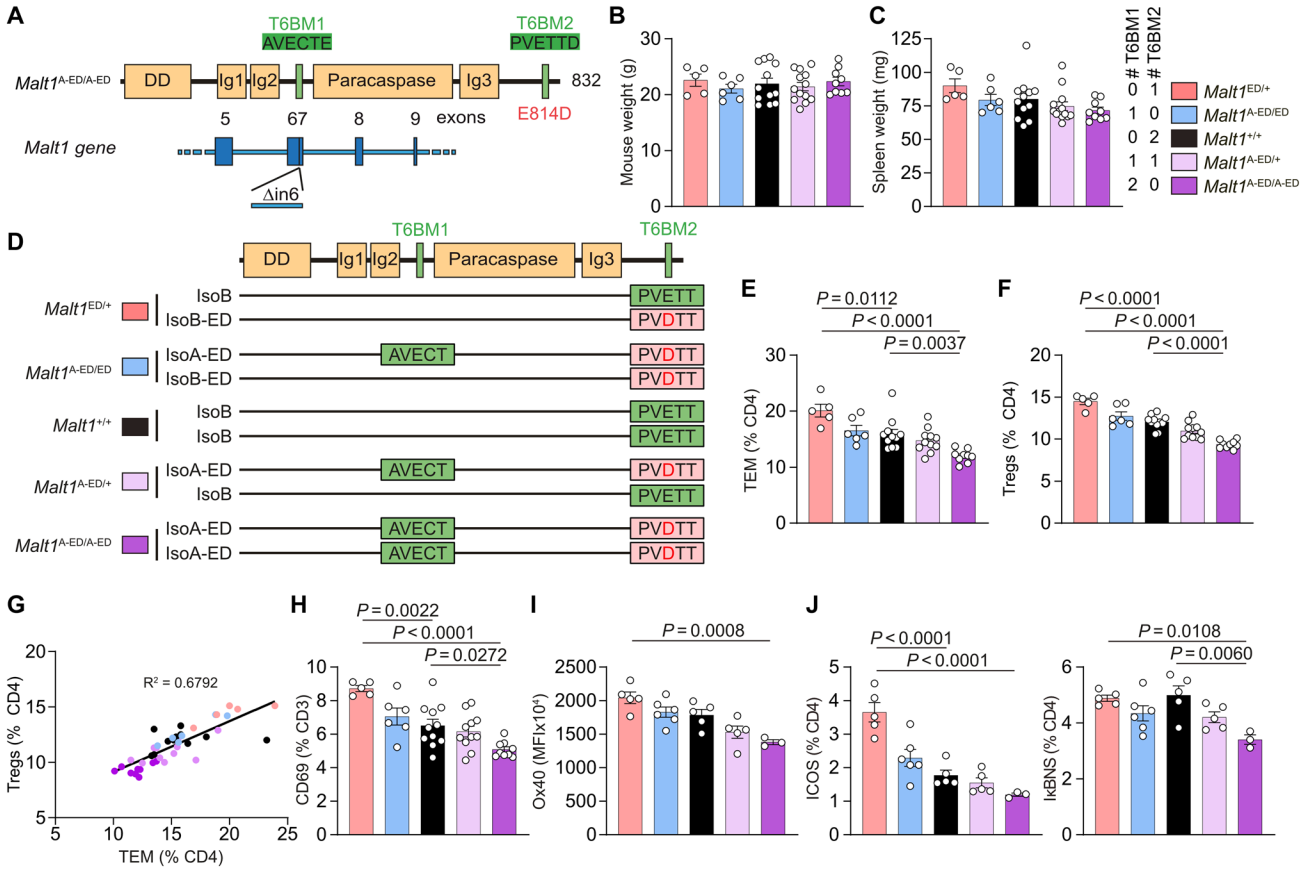

Fig. 6. Inflammation in *Malt1*$^{ED/ED}$ mice is rescued by enforced MALT1A expression. (**A**) Scheme of genomic alterations including *Malt1* T6BM2 E814D mutation in the context of *Malt1*$^{A/A}$ mice with exon 6/7 fusion (*Malt1*$^{A\text{-}ED/A\text{-}ED}$ mice). (**B** and **C**) Mouse (B) and spleen (C) weights of *Malt1*$^{ED/+}$ (pink), *Malt1*$^{A\text{-}ED/ED}$ (blue), *Malt1*$^{+/+}$ (black), *Malt1*$^{A\text{-}ED/+}$ (lavender), and *Malt1*$^{A\text{-}ED/A\text{-}ED}$ (purple) mice. (**D**) Scheme showing the number and locations of intact T6BMs in each genotype analyzed. (**E** to **G**) Percentages of CD4$^+$CD44^{hi}CD62L^{lo} effector memory T (T_{EM}) cells (E) and CD4$^+$FoxP3$^+$ regulatory T (T_{reg}) cells (F), and correlation of these populations (G). (**H**) Percentage of CD69$^+$CD3$^+$ T cells. (**I**) Mean fluorescence intensity (MFI) of Ox40 expression on CD4$^+$FoxP3$^+$ CD44^{hi}CD62L^{lo} effector T_{reg} (eTreg) cells. (**J**) Percentages of ICOS and IκBNS expression on splenic CD4$^+$ T cells. All analyses have been done using mice between 8 and 9 weeks after birth. $N = 5$ to 13 [(B), (C), (E), (F), and (H)] and 3 to 6 [(I) and (J)] for each group. Each dot represents one mouse. All bars show the mean ± SEM and *P* values were calculated by one-way ANOVA combined with Tukey's multiple comparisons test.

mice, *Malt1*$^{A\text{-}ED/A\text{-}ED}$ mice are viable and gain normal weight and subsequent analyses were performed at 8 to 9 weeks of age (Fig. 6B). Numbers of CD3$^+$ T and B220$^+$ B cells were within the normal range, and *Malt1*$^{A\text{-}ED/A\text{-}ED}$ mice do not develop splenomegaly or early symptoms of autoimmune inflammation to which *Malt1*$^{ED/ED}$ mice succumb at a young age (Fig. 6C and fig. S6A). Thus, enforced inclusion of exon 7 and MALT1A expression rescues the severe immune pathology caused by the disruption of the second T6BM, which affects MALT1B signaling and protease functions. However, *Malt1*$^{A\text{-}ED/A\text{-}ED}$ mice also did not show signs of immune deficiencies or autoimmunity associated with the destruction of the T6BM2 in humans (*16*).

While *Malt1*$^{A\text{-}ED/A\text{-}ED}$ mice express MALT1A E814D protein with an intact T6BM1 in all cells, *MALT1A* represents less than one-fifth of the total pool of *MALT1* in human hematopoietic cells and tissues (see Fig. 5A and fig. S3A). We wanted to more closely mimic the condition of the human MALT1 E806D patient and to explore the in vivo relevance of the number and positions of TRAF6 binding motifs, and thus the role of MALT1 alternative splicing for immune homeostasis. Therefore, we crossed *Malt1*$^{A\text{-}ED/+}$ mice with either *Malt1*$^{A\text{-}ED/+}$ or *Malt1*$^{ED/+}$ mice, the latter expressing exclusively MALT1B in immune cells. By combining the different *Malt1* alleles, we obtained mouse lines expressing either only one or two intact T6BM1 motifs (*Malt1*$^{A\text{-}ED/ED}$ or *Malt1*$^{A\text{-}ED/A\text{-}ED}$, respectively), one or two intact T6BM2 motifs (*Malt1*$^{ED/+}$ or *Malt1*$^{+/+}$, respectively), or one intact T6BM1 and one intact T6BM2 motifs (*Malt1*$^{A\text{-}ED/+}$) (Fig. 6D). Independent of the localization in MALT1, a single intact T6BM on one *Malt1* allele was sufficient to prevent the early-onset fatal autoimmune inflammation characterized by weight loss, splenomegaly, loss of CD3$^+$ and B220$^+$ B cells, massive expansion CD4$^+$ and CD8$^+$ T_{EM} cells, and up-regulation of activation marker CD69 observed in homozygous *Malt1*$^{ED/ED}$ mice (compare Figs. 2 and 6, B, C, E, F, and H, and fig. S6A). IκBα degradation after TCR/CD28 or P/I stimulation of CD4$^+$ T cells or P/I stimulation of CD19$^+$ B cells was normal, demonstrating that a T6BM from one allele and independent of its location in MALT1 can mediate a similar level of antigen receptor–induced NF-κB signaling (fig. S6, B and C).

Close inspection of T cell populations revealed that the shift from one intact T6BM in *Malt1*$^{ED/+}$ or *Malt1*$^{A\text{-}ED/ED}$ mice to two intact T6BMs in *Malt1*$^{+/+}$, *Malt1*$^{A\text{-}ED/+}$, and *Malt1*$^{A\text{-}ED/A\text{-}ED}$ mice coincided with a progressive reduction in the numbers of CD4$^+$ T_{EM} cells and, to a lesser extent, CD8$^+$ T_{EM} cells, and a decrease in the expression of the activation marker CD69 on CD3$^+$ T cells (Fig. 6, E

and H, and fig. S6D). Further, stepwise inclusion of more than one T6BM coincided with reduced frequencies of $CD4^+FoxP3^+$ T_{reg} cells (Fig. 6F). While numbers of eT_{reg} cells were not significantly altered, a gradual decline in expression of the suppressive marker OX40 was observed (Fig. 6I and fig. S6E). While two copies T6BM1 (*Malt1*$^{A\text{-}ED/A\text{-}ED}$) conferred the lowest $CD4^+$ T_{EM}/T_{reg} ratio, two copies of T6BM2 (*Malt1*$^{+/+}$) induced an intermediate ratio and only one copy of T6BM1 (*Malt1*$^{A\text{-}ED/ED}$) or T6BM2 (*Malt1*$^{ED/+}$) induced the highest ratio of $CD4^+$ conventional T_{EM} to T_{reg} cells (Fig. 6G). Thus, there was a linear correlation between the ratio of $CD4^+$ conventional T_{EM} to T_{reg} cells depending on not only the number but also the position of the T6BMs in MALT1. Accordingly, *Malt1*$^{ED/+}$ animals expressing one intact *Malt1* T6BM2 allele contain slightly more activated $CD69^+$ and T_{EM} cells as well as T_{reg} cells with augmented OX40 expression compared to *Malt1*$^{A\text{-}ED/ED}$ with one intact *Malt1* T6BM1 allele or *Malt1*$^{+/+}$ with two intact T6BM2 alleles (Fig. 6, H and I). The same trend in all parameters was apparent when comparing *Malt1*$^{+/+}$ mice with two intact *Malt1* T6BM2 alleles to *Malt1*$^{A\text{-}ED/A\text{-}ED}$ mice with two intact *Malt1* T6BM1 alleles. Consistently, *Malt1*$^{A\text{-}ED/+}$ mice containing one T6BM1 and one T6BM2 copy show an intermediate phenotype. Thus, expression of MALT1B with only the C-terminal T6BM2 leads to mildly enhanced T_{conv} cell activation and at the same time more suppressive T_{reg} cells under homeostatic conditions.

TRAF6 binding prevents constitutive MALT1 protease activity in resting T cells, thereby counteracting T cell effector differentiation through tonic TCR signaling (*6*). Using Western blotting, we have been unable to detect augmented constitutive MALT1 substrate cleavage in heterozygous *Malt1*$^{ED/+}$ mice (see Fig. 4E). Thus, we determined expression of NFKBID/IκBNS and ICOS, because both genes are controlled on the posttranscriptional level by MALT1-catalyzed cleavage of Roquin-1/2 and Regnase-1 (see Fig. 4, F and G) (*6*, *19*, *20*). In particular, ICOS expression on $CD4^+$ T cells is gradually increased by the removal of T6BMs with the highest expression in *Malt1*$^{ED/+}$ mice with only one intact T6BM2 (Fig. 6J). IκBNS is also increased particularly when comparing mice with two intact T6BM1s (*Malt1*$^{A\text{-}ED/A\text{-}ED}$) to one or two intact T6BM2s (*Malt1*$^{+/+}$ mice *Malt1*$^{ED/+}$). Thus, exon 7 inclusion and the presence of T6BM1 correlate with tighter regulation of targets controlled by MALT1-dependent Roquin-1/2 and Regnase-1 cleavage, which coincides with a reduction of conventional effector T cells as well as suppressive T_{reg} cells under homeostatic conditions.

Destruction of T6BM2 causes progressive autoimmune inflammation in aged *Malt1*$^{ED/+}$ mice

At a young age, heterozygous *Malt1*$^{ED/+}$ mice do not show any signs of immune disorders (see Fig. 2). However, we examined phenotypic changes in *Malt1*$^{ED/+}$ mice beyond 1 year after birth, to determine whether the mildly weakened immune homeostasis at a young age may progressively lead to autoimmune symptoms in older mice. Aged *Malt1*$^{ED/+}$ mice have normal body weight compared with litter- and cage-mate *Malt1*$^{+/+}$ controls (Fig. 7A). However, *Malt1*$^{ED/+}$ mice display significantly increased spleen weight (Fig. 7B). Numbers of $B220^+$ B and $CD3^+$ T lymphocytes were normal, with a mild skewing toward $CD4^+$ compared with $CD8^+$ T cells (Fig. 7, C and D, and fig. S6, F and G). In accordance with an immune activation phenotype, the population of conventional $CD4^+$ and $CD8^+$ T_{EM} cells was significantly increased and the activation marker CD69 was induced on the surface of $CD3^+$ T cells in *Malt1*$^{ED/+}$ mice (Fig. 7, E to G). As seen in young homozygous *Malt1*$^{ED/ED}$ mice, the number of T_{reg} and eT_{reg} cells as well as expression of OX40 on eT_{reg} cells was augmented in aged *Malt1*$^{ED/+}$ mice, suggesting the activation of counterbalancing immune-suppressive mechanisms (Fig. 7, H to J). B cells expressed higher levels of the activation markers CD69 and CD86, and an increased concentration of anti-dsDNA autoantibodies was detected in the serum of *Malt1*$^{ED/+}$ mice (Fig. 7, K to M). Furthermore, half of the *Malt1*$^{ED/+}$ mice showed increased concentrations of inflammatory TNF in the serum and high titers of anti-dsDNA antibodies correlated with high levels of TNF, indicating that chronic inflammation was induced beyond a certain threshold of autoantibodies (Fig. 7, M to O). Thus, only one intact *Malt1* T6BM2 allele leads to a progressively developing autoimmune inflammation in aged mice, reminiscent of the autoimmune disease in the homozygous *MALT1*$^{E806D/E806D}$ patient (*16*).

DISCUSSION

By engineering genetically modified mice to express an orthologous patient-derived MALT1 variant, we demonstrate that the single homozygous missense exchange MALT1 E814D in the C-terminal T6BM2 is sufficient to induce an early-onset acute immune pathology. Using blood analyses, we provide evidence that overshooting T and B cell effector responses induce autoimmune and inflammatory reactions that cause anemia, as evident from decreases in erythrocytes, hemoglobin, and hematocrit. The cause of this early-onset and rapidly progressing anemia is most likely multifactorial, involving humoral and cellular components. Mice with severe anemic conditions exhibit high blood markers that reveal liver damage, suggesting that progressive tissue destruction eventually necessitates euthanasia at around 3 weeks of age. Overall, *Malt1* E814D mice develop a fatal autoimmune inflammation that is highly reminiscent of *Malt1* TBM mice with complete destruction of both T6BMs (*6*). We have shown that *Malt1*$^{TBM/TBM}$ mice display severe tissue inflammation and multiorgan damage, which is associated with overshooting effector responses of conventional $CD4^+/CD8^+$ T cells, rather than a loss of suppressive functions of T_{reg} cells. Accordingly, conditional loss of MALT1-TRAF6 interaction in T_{reg} cells did not result in immune pathology (*6*). Of note, T_{reg} cell numbers are increased and T_{reg} cells are activated and up-regulate suppressive markers in both *Malt1*$^{ED/ED}$ and *Malt1*$^{TBM/TBM}$ mice. Thus, dysfunctional communication between conventional and suppressive T cells seems to contribute to the immune pathology, which may also be relevant for autoimmunity observed in aged heterozygous *Malt1* E814D mice.

The rapidly developing and fatal autoimmune inflammation of homozygous MALT1 E814D mice was unexpected, because in a human adolescent patient with the homozygous MALT1 E806D germline mutation, a severe but rather chronic immune syndrome with combined immune deficiency and autoimmunity has been previously described (*16*). In the murine setting, *Malt1*$^{ED/ED}$ mice phenocopy the immune pathology of *Malt1*$^{TBM/TBM}$ mice, in which mutation of both T6BMs leads to a complete abrogation of MALT1-TRAF6 interaction (*6*). Like *Malt1*$^{TBM/TBM}$ mice, all *Malt1*$^{ED/ED}$ animals necessitate euthanasia around 3 weeks of age, revealing that it is unlikely that the milder pathology of the MALT1 E806D patient is due to biological variations between individuals. Relative expression levels of alternative *MALT1* transcripts hint that slight differences in the abundance of *MALT1* isoforms account for the strong phenotypic variations caused by the defective MALT1 T6BM2 in mice and humans

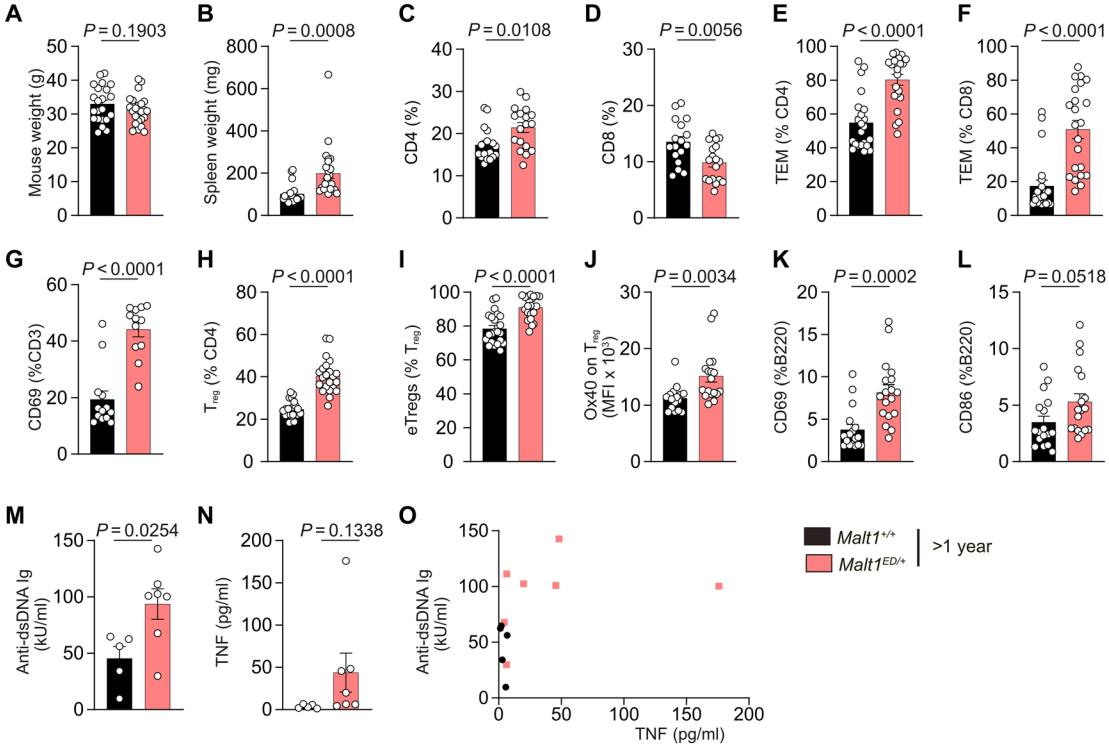

Fig. 7. Heterozygous *Malt1*$^{ED/+}$ mice develop autoimmune symptoms upon aging. Phenotypic analysis of *Malt1*$^{+/+}$ (black) and *Malt1*$^{ED/+}$ (pink) mice at >12 months. (**A** and **B**) Mouse (A) and spleen (B) weights. (**C** to **L**) Phenotypic analyses of lymphocytes in spleen of *Malt1*$^{+/+}$ and *Malt1*$^{ED/+}$ mice. [(C) and (D)] Relative numbers of CD4$^+$ (C) and CD8$^+$ (D) T cells. (E) Percentages of CD69$^+$ on CD3$^+$ T cells. [(F) and (G)] Relative numbers of CD4$^+$ (F) and CD8$^+$ (G) CD44^{hi}CD62L^{lo} effector memory T (T_{EM}) cells. [(H) and (I)] Relative numbers of CD4$^+$FoxP3$^+$ regulatory T (T_{reg}) (H) and CD4$^+$FoxP3$^+$ CD44^{hi}CD62L^{lo} effector T_{reg} (eTreg) cells. (J) Mean fluorescence intensity (MFI) of Ox40 on eT_{reg} cells. [(K) and (L)] Percentages of CD69$^+$ (K) and CD86$^+$ (L) on B220$^+$ cells. (**M** to **O**) Concentrations of anti-dsDNA immunoglobulin (M) and TNF (N) in the sera, with associated correlation (O). $N = 12$ to 24 [(A) to (L)] and 5 to 7 [(M) and (N)] for each group. Each dot represents one mouse. All bars show the mean ± SEM and P values were calculated by unpaired t test with Welch's correction.

(*3*). Even though *MALT1B* is the most abundant isoform across mammalian immune tissues and cells, the nearly complete absence of *MALT1A* mRNA and protein is a unique feature in the mouse immune system and not seen in humans. *Malt1*A is detected in most nonhematopoietic murine tissues, revealing no general inability for exon 7 inclusion in mice. The species-specific molecular mechanisms governing alternative splicing of MALT1 remain to be determined. Nevertheless, by introducing the MALT1 E814D mutation into *Malt1*$^{A/A}$ mice, which exclusively express MALT1A, we prove that inclusion of exon 7 and augmented MALT1A expression prevent the immune pathology of *Malt1*$^{ED/ED}$ mice. A single intact T6BM1 from one allele in heterozygous *Malt1*$^{A\text{-}ED/ED}$ animals is sufficient to rescue the early immune activation and lethality of *Malt1*$^{ED/ED}$ mice. Thus, our analyses uncover an unprecedented example of how species-specific regulation of alternative splicing directly affects the severity of a monogenetic disorder.

TRAF6 exerts a dual function for controlling antigen receptor signaling in T cells. Upon TCR/CD28 costimulation in activated T cells, TRAF6 binds to MALT1 in the context of the fully assembled CBM complex, thereby driving canonical NF-κB signaling in murine and human T cells (*6*, *22*). In addition, MALT1-TRAF6 interaction counteracts constitutive CBM activation in response to tonic TCR signaling in resting T cells, thereby preventing overshooting T cell activation in the absence of strong cognate antigens (*6*). By pharmacological MALT1 inhibition or genetic inactivation of MALT1 paracaspase, we previously demonstrated that uncontrolled MALT1 protease activity drives autoimmune inflammation upon loss of MALT1-TRAF6 binding or in the absence of TRAF6 (*6*, *23*). Further, the inability of Roquin-1 cleavage by MALT1 strongly ameliorates autoimmune inflammation in *Malt1* TBM mice (*24*). Defective MALT1 T6BM2 alone is sufficient to abrogate NF-κB signaling and induce chronic MALT1 protease activity in murine CD4$^+$ T cells. The phenotypic and mechanistic overlap of *Malt1* TBM and *Malt1* ED mice provides functional evidence not only that MALT1B is the predominant isoform in murine T cells, but also the autoimmune inflammation is triggered by uncontrolled MALT1 protease activation in both models.

Thus, the MALT1 T6BM2 mutation acts as a recessive hypomorph that affects only the function of MALT1B, and low expression of MALT1A (approximately $^1/_{10}$ of the total MALT1) in human immune cells is able to ameliorate the immune pathology. We have demonstrated that MALT1A E806D, with an intact T6BM1, can partially restore NF-κB activation on Jurkat T cells expressing MALT1B E795D mutation, but not to the same extent as MALT1A WT with two intact T6BM2 (*16*). Thus, the relative expression of MALT1A E806D to MALT1B E795D in T cells influences the severity of the biochemical effect of the mutation of the MALT1 T6BM2. Mechanistically, the effect of such a small proportion of MALT1A can only be understood in the context of the higher-order CBM complex (*25*–*27*). Preassembled BCL10-MALT1 heterodimers are recruited

as building blocks to the CARD11 seed, yielding oligomerization and formation of extended helical BCL10-MALT1 filaments. While, in murine T cells, the BCL10-MALT1 filaments are composed exclusively of MALT1B, approximately every 10th BCL10-MALT1 unit in human T cells contains MALT1A (~1:10 ratio MALT1A/MALT1B). Thus, in human T cells, destruction of MALT1 T6BM2 severely reduces but does not fully abolish TRAF6 binding. In humans, partial TRAF6 recruitment in the MALT1 E806D patient causes imbalanced signaling outputs with impaired NF-κB activation and augmented MALT1 protease activation, explaining the complex immune pathology with signs of immunodeficiency and autoimmunity (*16*). We provide evidence that the human autoimmune disease in the homozygous MALT1 E806D patient is more closely mimicked by heterozygous MALT1 E814D mice, which spontaneously develop autoimmunity and inflammation upon aging. However, NF-κB signaling in T and B cells from *Malt1*$^{ED/+}$ or *Malt1*$^{A\text{-}ED/ED}$ mice with one intact T6BM is normal, revealing no signs for immune deficiency. Of note, while, in T cells from heterozygous *Malt1*$^{ED/+}$ animals, every second MALT1 moiety contains an intact T6BM2, only every 10th MALT1A subunit in human T cells includes the intact T6BM1. This most likely explains the more severe immune pathology in the MALT1 E806D patient compared to the *Malt1*$^{ED/+}$ mice. Further complexity may arise from differences in MALT1A/MALT1B ratio in distinct immune cell subsets and on the single-cell level, which cannot be captured using current genetic mouse editing techniques. More importantly, the mouse models provide genetic evidence that the level of TRAF6 recruitment to MALT1 sets a signaling threshold for balancing immune homeostasis and activation.

By generating mice exclusively expressing either MALT1A (*Malt1*$^{A/A}$) or MALT1B (*Malt1*$^{B/B}$), we aimed to investigate the biological role of these alternative MALT1 transcripts. Despite a mild but sustained decrease in peripheral T_{reg} cells in mice expressing only MALT1A, *Malt1*$^{A/A}$ and *Malt1*$^{B/B}$ mice are phenotypically normal and do not show signs of disrupted immune homeostasis or changes in antigenic responses. Thus, despite the immune pathology caused by the destruction of MALT1 T6BM2, isoform-selective mouse models may be unable to uncover a physiological advantage of MALT1 alternative splicing. However, deleting either intron 6 or exon 7 also abrogates the dynamic control of MALT1 splicing. It is important to note the high evolutionary sequence conservation of MALT1 exon 7 not only on the protein level, but also on the level of the primary *MALT1* transcript and the secondary structure of the pre-mRNA in exon 7 and adjacent intronic regions, which recruits splicing factors hnRNP U and L to control exon 7 inclusion or skipping (*3*, *28*). Further, we did not observe an induction of *Malt1*A transcripts in *Malt1*$^{ED/ED}$ mice, which could prevent or at least ameliorate the devastating immune pathology. Thus, our data suggest a strong evolutionary pressure to maintain two MALT1 transcripts. At first glance, autoimmunity in aged heterozygous *Malt1*$^{ED/+}$ mice may suggest that it would be biologically favorable to abandon exon 7 skipping and only express MALT1A. However, especially in the immune system of mammals, there is obviously a selective pressure to retain MALT1B as the major isoform. We can only speculate about this conundrum. We observed a gradual decrease in conventional effector $CD4^+$ T cells, paralleled by a proportional decline in suppressive T_{reg} cells upon addition of T6BMs or a shift from an intact T6BM2 to an intact T6BM1. Homeostasis of $CD4^+$ T cell numbers relies on a quorum sensing–like mechanism, where interleukin-2 (IL-2) produced by activated $CD4^+$ T cells is sensed by high-affinity IL-2 receptors (CD25) on T_{reg} cells, and T_{reg} cells in turn can counterbalance the number of activated IL-2–producing $CD4^+$ T cells upon expansion (*29*, *30*). Dysregulation and alterations in the size of $CD4^+$ T cell pools may potentially predispose an organism to the development of immune disorders. We show that inclusion of MALT1 T6BM1 on exon 7 yields a lower number of both $CD4^+$ T_{EM} and T_{reg} cells, which may indicate that it confers a tighter immune regulation at the steady state and thus better protection from autoimmunity, but at the same time a decreased responsiveness to pathogens and infections. Accordingly, the sustained decrease in the numbers of peripheral T_{reg} cells in *Malt1*$^{A/A}$ mice may indicate a reduced need for peripheral immune tolerance mechanisms, because homeostasis of conventional effector T cells is more rigorously controlled by the addition of T6BM1 in MALT1A and the augmented recruitment of TRAF6 to the CBM complex. In contrast, MALT1B, as the predominant isoform in lymphocytes, seems to confer less stringent control of signaling homeostasis in T cells, thereby allowing for better antigenic responses, potentially at the expense of higher susceptibility to autoimmune reactions. We hypothesize that control MALT1A and MALT1B expression by alternative splicing of exon 7 reflects an evolutionary "trade-off" in balancing pathogen resistance over autoimmune prevention. While MALT1A may provide tighter control at the expense of optimal pathogenic immune activation, MALT1B seems to allow for better immune responses, but at increased risk of developing autoimmunity. Even though MALT1B is the predominant isoform in mammalian immune cells, the varying ratios of MALT1A to MALT1B indicate that discrete thresholds for this trade-off are set in different species. Many factors, such as genetic predispositions to autoimmunity, pathogenic and environmental exposures, or life expectancy may influence how this ratio is set in each species and potentially in specific tissues or cells.

Allogenic hematopoietic stem cell transplantation (HSCT) has been effective for normalizing immune functions, especially in young patients with confirmed germline MALT1 deficiency (*31*–*33*). Thus, HSCT seems a viable option for curative treatment of the MALT1 E806D patients or other patients characterized by defective MALT1-TRAF6 interaction (*16*). Future strategies may also envision gene editing of patient HSCs to either directly correct the inborn error or modulate MALT1 splicing, which would allow autologous transplantation with potentially less adverse effects. Alternatively, potent and selective MALT1 inhibitors have been developed and are currently in evaluated in early clinical trials for the treatment of aggressive lymphomas (*34*). In mice, pharmacological MALT1 inhibition ameliorates autoimmune inflammation caused by TRAF6 deficiency in T cells (*6*), revealing that MALT1 targeting can be a feasible strategy to treat autoimmune patients characterized by a loss or reduction of MALT1-TRAF6 interaction, especially if they are not eligible for HSCT. Of note, genetic TRAF6 variants are associated with higher risks for rheumatoid arthritis and systemic lupus erythematosus (*35*, *36*). Given the tight control of MALT1 protease by TRAF6, it would be of particular interest if MALT1 protease inhibition could be used to treat autoimmunity on a broader scale in older patients. However, MALT1 inhibition has been shown to deplete T_{reg} cells, which, upon long-term treatment, causes severe complications such as intestinal inflammation in animal models (*6*, *37*). Thus, intermittent dosing may be an option to balance the beneficial and adverse effects of MALT1 inhibitors in the treatment of autoimmune diseases.

Together, cross-species comparisons of a rare *MALT1* variant that disrupts TRAF6 binding to the MALT1B isoform uncovers that MALT1 splicing and TRAF6 recruitment functions as a molecular rheostat for balancing immune homeostasis and activation. On the basis of human genome databases, we demonstrate that more genetic *MALT1* variations exist, which cause loss of TRAF6 binding to MALT1B, thereby impairing NF-κB signaling while inducing MALT1 protease activity to the same extent as the *Malt1* E806D mutation. Our data indicate that even in a heterozygous setting, such mutations can cause an imbalance of MALT1 scaffolding and protease regulation, and it will be interesting to see whether the resulting weakening of immune homeostasis can predispose human carriers to the development of autoimmunity.

MATERIALS AND METHODS

Study design

The aim of this study was to characterize molecular and cellular mechanisms regulating immune signaling pathways that are affected by the patient germline mutation MALT1 E806D, resulting in a complex immune disorder with symptoms of immune deficiency and autoimmunity. To phenocopy the human pathological condition, the genetically modified mouse line *Malt1* ED was generated carrying the orthologous MALT1 E814D mutation. Mice were phenotypically analyzed using flow cytometry, cytokine analyses, hematological and clinical chemistry analyses, and ex vivo analyses of T cell signaling by Western blot and flow cytometry.

For profiling *Malt1A* and *Malt1B* splice isoform expression in mice and men, expression databases and qualitative and quantitative RT-PCR from primary immune cells were used, and a MALT1A-specific antibody was developed. To further investigate the biological relevance of *Malt1* alternative splicing, two additional mouse lines expressing exclusively either MALT1A or MALT1B were generated and phenotypically characterized. The *Malt1* IsoA mouse line was further used to generate the *Malt1* A-ED line, which contains the E814D mutation in the exclusively expressed *Malt1A* isoform to study the impact of alternative splicing on the pathological outcome of the E814D mutation. Age-matched littermates with equivalent genetic background were used. Reported phenotypes remained reproducible for at least eight generations.

Generation of mouse lines via CRISPR-Cas9–based gene editing

Animal experiments were conducted in accordance with the German animal welfare law and the guidelines of the Federation of European Laboratory Animal Science Association. Animal experiments were performed with permission and in accordance with all relevant guidelines and regulations of the district government of Upper Bavaria (Bavaria, Germany; Animal protocol numbers ROB-55.2-2532-VET_02-17-122, ROB-55.2-2532-VET_02-22-111, and ROB-55.2Vet-2532.Vet_03-17-68).

The *Malt1* ED mouse line was generated by CRISPR-Cas9–based gene editing of one-cell embryos. A specific single guide RNA (sgRNA) targeting TRAF6 binding motif 2 (T6BM2) in MALT1 [Malt1_E814D_gRNA: 5′-CATCTCTGTTGACTACTTTA-3′; designed as previously described (*6*)] was produced by in vitro transcription (EnGen sgRNA Synthesis kit, NEB, E3322). To introduce the homologous patient-derived T6BM2 mutation in exon 17 of Malt1, a short single-stranded oligodeoxyribonucleotide (ssODN) HDR template (ssODN_Malt1_E814D: 5′-CCAGACAGGTGTCATTGCAGCCGGACTCCACACACATTCATTTCAAATTATCCCCCCCACCACTACTGCCAGTTTGGTAGATCCAATGTGCCCGTGGACACGACCGACGAAATGCCATTCAGTTTTTCTGACAGGCTTATGATTTCTGAAAACTGACCTTCATGGTTTTGAAAATTAGAATAGTTACAGTAATCT-3′) was synthesized. Additional silent mutations in the region of the T6BM2 mutation allow identification of targeted alleles via differential PCR amplification using WT- and mutation-specific primers. sgRNA (200 ng/μl) and ssODNs (300 ng/μl) were electroporated together with recombinant Cas9 protein (200 ng/μl, IDT) into one-cell embryos using an NEPA21 electroporator and a CU-Y501P1-1.5 electrode (Nepa Gene Co). Zygotes were transferred into pseudopregnant CD1 female mice to obtain live pups. Gene-editing events were analyzed on genomic DNA isolated from ear biopsies of founder mice and F1 progeny using the Wizard Genomic DNA Purification kit (Promega, A1120) following the manufacturer's instructions. Modification of T6BM2 was detected via genotyping using WT- and mutation-specific primers (T6BM2 fwd general: 5′-ACGGATAAGAGTGGAGTGAT-3′; T6BM2 rev WT-specific: 5′-ATTTCATCAGTTGTCTCT-3′; T6BM2 rev Mut-specific: 5′-ATTTCGTCGGTCGTGTCC-3′) and verified by sequencing.

Malt1 IsoA mice were generated by CRISPR-Cas9 mutagenesis in R1/E (129S1/X1) ES cells using an optimized protocol (*38*). *Malt1* exons 6 and 7 were fused by deleting intron 6 using a CRISPR guide (5′-atataagctgcatacactgg-3′, located within intron 6) and a linear 1650-bp double-stranded DNA homology template (synthesized by Geneart, Regensburg, Germany) for HDR. Single ES cell clones were screened to identify mutant alleles using PCR primers specific for correct genomic insertion of the HDR template (fwd primer upstream of the HDR template: 5′-ctcagaatccaggttgcaaatct-3′ and rev primer specific for the exon 6/7 fusion region: 5′-CTGCCTCATCTGTTCTTCCTATG-3′). In the selected ES cell clones, genomic modifications were confirmed by sequencing. The ES cell clone containing correct homozygous alterations was injected into eight-cell C57BL/6Ncrl WT embryos by using laser-assisted injection technology (*39*). A total of 10 to 12 embryos were transferred into the oviduct of a pseudogravide Crl:CD1(IDR) female, and chimeric males were born with brown fur (>90% chimerism). After crossing C57BL/6NCrl animals, germline transmission and brown F1 generation yielded heterozygous Malt1 IsoA/+ (A/+), which were further backcrossed to the C57BL/6NCrl background for at least eight generations. The complete *Malt1* CDS was sequenced to verify that no additional mutations changing the coding sequence were found (fig. S4A). IsoA mice were genotyped by PCR using a common fwd primer A1 (5′-TTAATGAATGATGATGATTTAAGGATG-3′) together with a WT-specific rev primer A2 (5′-ACTCCAAAACCACATAACTCACA-3′) and an IsoA specific rev primer A3 (5′-CTCATCTGTTCTTCCTATGGTG-3′), which, upon annealing at 58°C, result in a 625-bp band, indicating the WT allele and a 255-bp band indicating the IsoA allele (fig. S4A).

For generating *Malt1* IsoB mice, Malt1 exon 7 was deleted by CRISPR-Cas9 directly in mouse zygotes by using two CRISPR guides flanking exon 7. Sperm from C57BL/6NCrl male mice was used for in vitro fertilization in C57BL/6NCrl females (obtained from Charles River, Sulzbach, Germany) superovulated with 5 U of PMSG (Pregnant Mare's Serum Gonadotropin) and 5 U of HCG (Human Chorionic Gonadotropin). Fertilized one-cell embryos were edited by electroporation using specific in vitro transcribed (EnGen sgRNA

Synthesis Kit, NEB, E3322, USA) single gRNAs (5′-GCTTAGATAACATGATTCTG-3′ and 5′-ATCACTGCACGTAGTGAGCT-3′). Before electroporation, the sgRNAs (200 ng/μl) were diluted in Opti-MEM buffer (Thermo Fisher Scientific, Germany) together with recombinant Cas9 protein (200 ng/μl, IDT, Coralville, USA) and incubated for 10 min at room temperature (RT) and 10 min at 37°C to form the active ribonucleoprotein complex.

Electroporation was performed using the NEPA21 electroporator and a CUY501P1-1.5 electrode (Nepa Gene Co. Ltd., Japan). Zygotes were transferred into pseudopregnant CD1 female mice to obtain live pups. Deletion of exon 7 in offspring mice was detected via PCR (fwd: 5′-GATCAGCATTCCCTATTGTGAG-3′ and rev: 5′-GAGAAACTCTATGGGTCTTATG-3′) and verified by sequencing (fig. S4B). IsoB mice were genotyped by PCR using fwd primer B1 (5′-GTGAGTTATGTGGTTTTGGAGT-3′) and rev primer B2 (5′-GACGACCTATTAGAGCTAGTATT-3′), which, upon annealing at 58°C, result in a 354-bp band indicating the WT allele and a 148-bp band indicating the IsoB allele (fig. S4B).

For the generation of *Malt1* A-ED mice, *Malt1* IsoA males were mated with 4-week-old superovulated C57BL6/NCrl females. The next morning, the fertilized eggs were removed from the fallopian tube in the cumulus complex, isolated with hyaluronidase, and then washed. The eggs were then electroporated with ssODN HDR template as depicted for *Malt1* ED mice and recombinant Cas9 protein to generate *Malt1* E814D mutation using Bio-Rad Gene Pulser Xcell Electroporator (two pulses of 3 ms at 30 V) as described previously (*40*). Genotyping and crossing to generate *Malt1* A-ED mice have been performed as described above.

Immune cell phenotyping by flow cytometry

Lymphocyte populations were analyzed from single-cell splenocyte suspensions derived from spleens or lymph nodes. Organs were meshed and subjected to RBC lysis (Miltenyi Biotec, 130-094-183), and 1×10^6 cells were used per staining. Cells were washed twice with phosphate-buffered saline (PBS; 350*g*, 5 min, 4°C), and dead cells were stained with eFluor780 live/dead cell permeable dye (eBioscience, 65-0865-18, 1:1000 in PBS, 30 min, 4°C). Cells were washed with FCM buffer [3% fetal bovine serum (FBS) in PBS] and treated with anti-CD16/CD32 (Fc-block, eBioscience, 14-0161-85, 1:200 in FCM buffer, 20 min, RT). Supernatant was discarded and cells were stained with the following fluorescent-coupled antibodies (in FCM buffer, 20 min, RT): anti-CD3-PECy7 (25-0031-82, 1:300), anti-CD45R-PerCP-Cy5.5 (BioLegend, 103234, 1:200), anti-CD8a-FITC (11-0081-85, 1:100), anti-CD4-PE (12-0042-85, 1:300), anti-CD4-PerCP-Cy5.5 (45-0042-82, 1:300), anti-CD44-PECy7 (25-0441-82, 1:400), anti-CD44-FITC (11-0441-81, 1:300), anti-CD62L-APC (BD Pharmingen, 553152, 1:300), anti-CD86-FITC (11-0862-82, 1:100), anti-CD69-APC (17-0691-82, 1:200), anti-Ox40-PECy7 (25-1341-80, 1:200), anti-CTLA-4-PECy7 (BioLegend, 106313, 1:200), anti-CD19-APC (Elabscience, E-AB-F0986UE, 1:200), and anti ICOS-FITC (11-9949-82, 1:200). All antibodies are from eBiosciences except where indicated. For intracellular staining of FoxP3, cells were permeabilized and fixed (eBiosciences, 00-5223-56), washed once with permeabilization buffer (eBiosciences, 00-8333-56), and stained with anti-FoxP3-PE (12–5773-82, 1:100 in permeabilization buffer, 30 min, RT). Cells were washed with FCM buffer and analyzed using an Attune Acoustic Focusing Cytometer (Thermo Fisher Scientific) or a FACS Canto II Flow Cytometer (Becton Dickinson).

Analysis of intracellular protein expression by flow cytometry

For intracellular staining of IκBNS or IκBα, 1×10^6 cells were either left untreated or stimulated with P/I or anti-CD3/28 (Dynabeads according to manufacturer's protocol) for 30 min. Cells were washed twice with PBS (350*g*, 5 min, 4°C) and stained with eFluor780 live/dead cell permeable dye (eBioscience, 65-0865-18, 1:1000 in PBS, 30 min, 4°C). Cells were fixed in 2% paraformaldehyde (15 min, RT) and permeabilized in saponin buffer [0.5% saponin and 1% bovine serum albumin (BSA) in PBS, 20 min, RT]. Cells were incubated with anti-CD16/32 (1:100 in saponin buffer, 15 min, 4°C) and then stained with either anti-IκBNS antibody (clone 4C1, RRID: AB_3695855, 1:10 in saponin buffer, 30 min, 4°C) or intracellular anti–IκBα-PE (Cell Signaling Technology, 7523, 1:100). For IkBNS-stained samples, cells were washed once with saponin buffer and stained with goat anti-rat IgG-AF647 secondary antibody (BioLegend, 405416, 1:200 in saponin buffer, 30 min, 4°C), while IκBα-stained samples were washed once with saponin buffer and stained with goat anti-rat IgG-AF647 secondary antibody (BioLegend, 405416, 1:200 in saponin buffer, 30 min, 4°C). Cells were washed twice with saponin buffer and the second wash was incubated for >15 min at RT to wash out unbound antibodies. For surface staining of IκBNS-stained samples, cells were incubated with anti-CD4 (1:300), anti-CD8 (1:100), and anti-ICOS (1:200, all in saponin buffer, 30 min, RT). All samples were washed with saponin buffer, resuspended in FCM buffer, and acquired on an Attune Acoustic Focusing Cytometer (Thermo Fisher Scientific).

Analysis of EDTA-blood and blood plasma

Blood from the submandibular vein of mice was collected in tubes coated with 0.5 M EDTA (pH 8.0) and containing 2 μl of 0.1 M EDTA. Blood and anticoagulant were gently mixed and an additional 0.1 M EDTA was added to obtain a final concentration of 5 mM EDTA. EDTA whole blood was diluted 1:7 with Cellpack DCL diluent (Sysmex) and briefly vortexed. Blood parameters were measured on a Sysmex XN-9100. The remaining EDTA whole blood was centrifuged (650*g*, 10 min, 4°C). Clear blood serum was transferred to a new tube and diluted 1:4 with PBS. Clinical parameters were measured on a cobas 8000 modular platform (Roche) using ALTPM (05531462190), ASTPM (05531446190), GLDH3 (11929992 216), and LDHI2 (05169330 190, all from Roche).

Analysis of cytokines and autoantibodies

Cytokines in sera of mice were measured according to the manufacturer's protocol via flow cytometry using a cytometric bead array kit (BD, 562246) and specific beads for IFN-γ (562233) and TNF (562336). Autoantibodies in serum of mice were measured according to the manufacturer's protocol via enzyme-linked immunosorbent assay (ELISA; Alpha Diagnostic International, 5110).

Stimulation of primary murine cells

Splenocytes were stimulated with PMA (Calbiochem, 524400-1, 200 ng/ml)/ionomycin (Iono, Calbiochem, 407950-1, 300 ng/ml) or anti-CD3 (BD, 553057, 0.5 μg/ml)/-CD28 (553294, 1 μg/ml) on rabbit anti-hamster IgG (Dianova, 307-005-003) precoated plates. Keratinocytes were stimulated with P/I as described below.

Isolation and cultivation of primary murine keratinocytes from neonatal skin

Primary murine keratinocytes were isolated from neonatal skin of 1- to 2-day-old pups. Mice were euthanized by decapitation, and

bodies were rinsed in 80% ethanol. Limbs and tail were removed and the skin was cut from the tail hole along the dorsal midline of the body to the opening of the neck. The whole skin was peeled off the body and rinsed in PBS (without Ca^{2+}). The skin was incubated with ice-cold dispase II digestion buffer [dispase II (4 mg/ml; Sigma-Aldrich, D4693) in KC growth medium (PromoCell, C-20111), overnight, 4°C, rotating]. After 12 to 18 hours of incubation, the skin was washed in PBS to remove dispase II. To separate dermis and epidermis, the skin was placed with the dermis side up in an empty dish and the dermis was lifted up and away from the epidermis by using forceps. The epidermis was transferred to a dish containing 500 µl of TrypLE Express enzyme (Thermo Fisher Scientific, 12604013) and floated on top of the solution with the basal layer downward for 20 min at RT on a shaker with gentle agitation. To release single cells from the epidermal sheet, 2 ml of KC growth medium was added, and the epidermis was rubbed back and forth using forceps. The cell suspension was collected and transferred to a 50-ml Falcon tube. This procedure was repeated two more times and cell suspensions were combined. To break cell clumps, cell solution was pipetted up and down several times and passed through a 100-µm filter into a new 50-ml Falcon tube. Cells were centrifuged (180*g*, 5 min, 4°C), resuspended in 1 ml of cold KC growth medium, and placed on ice to avoid spontaneous differentiation. Cells were seeded in six-well plates, precoated with attachment factor protein (Thermo Fisher Scientific, S006100) at a density of 0.5×10^6 to 1×10^6 cells per well and cultured in humidified atmosphere (37°C, 5% CO_2). Twenty-four hours after plating, medium was changed to remove unattached cells. Medium was changed every 2 days until cells reached the desired confluency.

Isolation of primary human or murine PBMCs from blood

For work with human PBMCs and $CD4^+$ T cells, ethical approval was obtained from the Institutional Review Boards: no. 2025206-S-SB (Ethikkommission, Technische Universität München). All blood donors provided written informed consent. All work was carried out in accordance with the Declaration of Helsinki for experiments involving humans.

For isolation of primary human PBMCs, blood from donors was collected in lithium heparin monovettes (Sarstedt, 02.1065.001). Blood was centrifuged (300*g*, 10 min, RT, no break) and the intermediate buffy coat layer containing leukocytes and platelets was collected and diluted with PBS up to a total volume of 35 ml. To isolate mononuclear cells (MNCs), diluted buffy coat was carefully layered onto 15 ml of Lymphoprep density gradient medium (STEMCELL Technologies, 07801) and centrifuged (160*g*, 20 min, RT, no break). About 20 ml of the supernatant was removed and the sample was centrifuged again (350*g*, 20 min, RT, no break). Last, the intermediate layer containing the MNCs was transferred and washed two times with PBMC buffer [0.1% BSA and 2 mM EDTA (pH 7.4) in PBS; 300*g*, 8 min, 4°C]. MNCs were resuspended in RPMI 1640 supplemented with 10% FBS, penicillin (100 U/ml), 100 µg streptomycin (all Gibco), and 50 µM β-Mercaptoethanol (Roth).

For isolation of primary murine PBMCs, blood from the submandibular vein of mice was collected in EDTA-coated tubes and pooled to have a total volume of 1 ml. Blood was diluted with 1 ml of PBS (+2% FBS) and layered onto 1.5 ml of Lymphoprep density gradient medium. After centrifugation (800*g*, 20 min, RT, no break), the upper plasma layer was removed and MNCs were transferred and washed two times with PBS (+ 2% FBS; 400*g*, 4 min, 4°C).

Preparation of whole cell lysates

Total splenocytes or keratinocytes (3×10^6 to 10×10^6) were lysed in coimmunoprecipitation buffer [25 mM Hepes, pH 7.5, 150 mM NaCl, 0.2% NP-40, 10% glycerol, 1 mM DTT, 10 mM NaF, 8 mM β-glycerophosphate, 300 µM sodium vanadate, and protease inhibitor cocktail mix (Roche)] for 20 min at 4°C. Lysates were centrifuged (20,000*g*, 12 min, 4°C) and supernatant was mixed with 4× SDS loading buffer and boiled for 5 min at 95°C. Lysates were separated by SDS–polyacrylamide gel electrophoresis (SDS-PAGE) and analyzed by Western blot.

Western blotting

To transfer SDS-PAGE separated proteins onto PVDF membranes, an electrophoretic semidry blotting system was used (Merck Millipore, IPVH00010). After transfer, membranes were blocked with 5% milk (Roth, T145.1) in PBS-Tween (0.01% Tween) (1 hour, RT). Primary antibodies were diluted as indicated in 2.5% BSA (Sigma-Aldrich, A7906) or milk in PBS-T and membranes were incubated overnight at 4°C. Membranes were washed three times with PBS-T for 10 min and treated with horseradish peroxidase (HRP)–coupled secondary antibodies (Jackson ImmunoResearch, 1:5000 in 1.25% BSA or milk in PBS-T) (1 hour, RT). HRP was detected by enhanced chemiluminescence using the LumiGlo reagent kit (Cell Signaling Technologies, 7003) according to the manufacturer's protocol and visualized on ECL Amersham Hyperfilms (GE Healthcare, 28906837). The following Western blotting (WB) antibodies were used: anti-IκBα (L35A5), anti-p65 (D14E12), and anti-p-p65 (93H1) (all Cell Signaling Technology); anti-MALT1 (D-1), anti-β-Actin (C4, 1:20.000), anti-CYLD (E-10), and anti-HOIL-1 (H-1) (all Santa Cruz); anti-N4BP1 (EPNCIR118, Abcam); and anti-Regnase-1 (R&D Systems, MAB7875); all antibodies were used at 1:1000 dilution if not otherwise stated.

Analysis of MALT1A and MALT1B splice isoforms

For analysis of MALT1 splicing, total splenocytes/PBMCs or magnetic cell separation (MACS)-purified CD4 T cells were used (Miltenyi Biotec, 130-096-533 or 130-104-454). For RNA isolation and cDNA synthesis, primary murine or human cells (1×10^7) were collected and washed with PBS (350*g*, 5 min, 4°C). Cells were resuspended in 600 µl of Trizol (Thermo Fisher Scientific, 15596018), briefly vortexed, and incubated for 5 min at RT. After adding 120 µl of Roti-Phenol/Chloroform/Isoamylalcohol (Roth, A156) and shaking vigorously by hand for 15 s, cells were incubated for 3 min at RT and centrifuged (18,000*g*, 5 min, 4°C) to separate phases. The colorless upper aqueous phase was transferred to a new tube, and an equal volume of 80% ethanol was added and mixed by pipetting up and down. RNA was applied to columns (RNeasy Mini Kit, Qiagen, 74106) and further purified according to the manufacturer's instructions. RNA was reverse transcribed into cDNA using the Verso cDNA Synthesis Kit (Thermo Fisher Scientific, AB1453B) according to the manufacturer's protocol.

Samples were adjusted to RNA input equivalents (5 ng/µl; e.g., if 500 ng of input RNA was used for reverse transcription, the resulting cDNA was taken up in 100 µl of total volume). cDNA (5 µl) was used as template in qRT-PCR. For generation of standard curves, plasmids containing either the *MALT1* IsoA or IsoB cDNA sequence were serially diluted to various concentrations (copy numbers per microliter) and 5 µl of the dilutions was used as standards in qPCR. Individual PCRs were run using hMALT1 IsoB forward

(AAGCCCTATTCCTCACTACCAGTGG) and reverse (GGATGACCAAGATTATTTAATTCATCTATG) and hMALT1 IsoA forward (5′-GAAGGTAGAAATCATCATAGGAAG) and reverse (5′-GCTTTGAGCTTGGGGTGCTCC) primers for PCR with SYBRgreen mastermix (Takyon). Data were analyzed using the Lightcyler 480 Software. From the standard values, standard curves were generated by linear regression, and from this, copy numbers of the donor samples were determined for IsoA and IsoB and eventually IsoA/B ratios were calculated. For murine samples, RNA was isolated from WT, *Malt1*$^{A/A}$, or *Malt1*$^{B/B}$ mice and RNA and cDNA were prepared as described above. cDNA (5 μl) was used as template in RT-PCR using MALT1 ex5 forward (5′-CCCTATTCCTCACTACCAGTG) and MALT1 ex10 reverse (5′-CCCGGTAATTCATATTTCCTATC) primers. The RPII control PCR was run using forward (5′-GCTCCATTGCTGCCAACATGAC) and reverse (5′-CACATGTGCCGTTCCACCTTATAGC) primers.

For the human competitive PCR, Malt1 ex5 forward (5′-CCCTATTCCTCACTACCAGTG) and Malt1 ex10 reverse (5′-CCCGGTAATTCATATTTCCTATC) primers were used. For murine competitive PCR, MALT1 ex6 forward (5′-ACCGAGACAGTCAAGATAGC) and MALT1 ex9/10 reverse (5′-GACTTTGTCCTTTGCCAAAGG) primers were used. For the RPII control PCR, forward (5′-GCTCCATTGCTGCCAACATGAC) and reverse (5′-CACATGTGCCGTTCCACCTTATAGC) primers were used together with Herculase II polymerase (Agilent, 600675).

In vitro binding of MALT1 T6BM to TRAF6

HIS-TRAF6$_{310–522}$, GST-MALT1$_{286–346}$ (T6BM1), or GST-MALT1$_{764–824}$ (T6BM2) was purified on an ÄKTA purifier system using 1-ml HisTrap and GSTrap columns (GE Healthcare, GE17-5247-01 and GE17-5281-01). Proteins were further purified over a size exclusion column (GE Healthcare, Superdex 75 10/300 GL, 17-5174-01). To detect in vitro binding of TRAF6 to MALT1 T6BMs, AlphaScreen was performed according to the manufacturer's protocol. Briefly, in a 96-well plate, 100 nM HIS-TRAF6$_{310–522}$ was incubated together with 100 nM GST-MALT1$_{286–346}$ (T6BM1; WT) or GST-MALT1$_{764–824}$ (T6BM2; WT, E806A or E806D) in AlphaScreen buffer (1× PBS, 0.5% BSA, 0.01% Tween 20) for 1 hour at RT. Glutathione donor (Revvity, 6765300) and nickel-chelate acceptor beads (Revvity, 6760619C) were added and incubated for 1 hour at RT in the dark. Chemiluminescence was measured on an Envision 2104 plate reader (PerkinElmer). Results from WT and mutant binding were normalized to relative WT controls, and K_d was calculated in GraphPad Prism by nonlinear curve fit with Hill slope.

Generation of MALT1A 4A7 antibody

A MALT1 IsoA-specific monoclonal antibody was generated by immunization of Lou/c rats with ovalbumin-coupled peptide GRTDEAVECTEDELNN spanning exon 7 and exon 8 of human/mouse MALT1 (Peps4LS, Heidelberg). Animals were injected subcutaneously and intraperitoneally with a mixture of 40 μg of peptide, 5 nmol CpG (Tib Molbiol, Berlin, Germany), and an equal volume of incomplete Freund's adjuvant. A boost injection was given 12 weeks later without Freund's adjuvant and spleen cells were fused with P3X63Ag8.653 myeloma cells using polyethylene glycol 1500 according to standard procedure (*41*). Hybridoma supernatants were screened in a solid-phase ELISA for binding to his-tagged biotinylated peptide coated to streptavidin plates. Positive supernatants were further validated by immunoblot analysis. Hybridoma cells from selected supernatant were subcloned twice by limiting dilution to obtain the stable monoclonal cell clone MLT1A 4A7 (RRID AB_3713424). Experiments were performed with hybridoma supernatant and a mouse–anti-rat IgG2c secondary antibody (R2C 1F8, in-house).

CD4$^+$ T cell proliferation assay

CD4$^+$ T cells were MACS purified from splenocytes using the CD4$^+$ T Cell Isolation Kit (Miltenyi Biotec, 130-104-454) according to the manufacturer's protocol. MACS-purified CD4$^+$ T cells were carboxyfluorescein succinimidyl ester (CFSE) labeled with 5 μM CFSE in PBS for 10 min (CFSE Cell Division Tracker Kit, BioLegend, catalog no. 423801). One hundred thousand CFSE-labelled CD4$^+$ T cells were then stimulated with plate-bound CD3 (coated at 0.5 μg/ml in 100 μl PBS per well for 3 hours at RT, hamster CD3e antibody, clone 145-2C11, BD Pharmingen, catalog no. 553057, RRID:AB_394590) and soluble CD28 (1 μg/ml, hamster CD28 antibody, clone 37.51, BD Pharmingen, catalog no. 553294, RRID:AB_394763) in 96 well-plates (Corning Costar CLS3997) which were coated for 16 hours at 4°C with cross-linking antibody (5 μg/ml in PBS, anti-Syrian Hamster IgG (H + L), Jackson ImmunoResearch, Cambridgeshire, UK, 307-005-003, RRID: AB_2339572). Unstimulated cells served as controls. Cells were incubated at 37°C, 5% CO_2 for 3 days (or the time indicated).

For flow cytometric analysis of CFSE proliferation, cells were incubated with eBioscience fixable viability dye eFluor 780 (Thermo Fisher Scientific, cat: 65-0865-18) and then cells were measured on an Attune Acoustic Focusing Flow Cytometer using the BL-1 channel for CFSE and the RL-3 channel for eFluor 780. Data were further processed using FlowJo Software (BD Biosciences). For more details, see the Supplementary Materials.

Mouse immunization

Mice were immunized intraperitoneally at an age of 8 to 10 weeks with 100 μg of NP-Ova in Alum. Mice were bled at indicated days after immunization for measuring NP-specific immunoglobulins in blood serum.

NP-specific immunoglobulin IgG1 or IgM concentrations were measured by ELISA (SBA Clonotyping System-AP, SouthernBiotech, no. 5300-04 and Mouse Immunoglobulin Panel, SouthernBiotech, catalog no. 5300-01). ELISAs were developed with PNPP (Thermo Fisher Scientific, 34047) measuring absorption at 405 nm with an Envision 2104 plate reader (PerkinElmer). The blank absorption value was subtracted from all other absorption values, and the IgG1 or IgM standard curves were generated and used within its linear range to calculate the NP-specific serum concentrations. For more details, see the Supplementary Materials.

Statistics and reproducibility

For mouse studies, statistical design and replications were performed as mandatory for legal approval for animal experimentations. Statistical analyses and data visualization were performed in GraphPad Prism versions 8.0 and 10.0. Number of biological replicates and all details on statistical tests are provided in each figure legend. All quantification and statistical analyses have been done on at least three biological replicates. Values represent the means ± SEM as indicated in the figure legends. Exact *P* values are depicted in the figures. Nonspecific (ns) *P* values ($P \geq 0.05$) are not shown unless pertinent.

Supplementary Materials

The PDF file includes:

Supplementary Materials and Methods
Figs. S1 to S7
Legend for data S1

Other Supplementary Material for this manuscript includes the following:

Data S1

REFERENCES

1. M. Juilland, M. Thome, Holding all the CARDs: How MALT1 controls CARMA/CARD-dependent signaling. *Front. Immunol.* **9**, 1927 (2018).
2. J. Ruland, L. Hartjes, CARD-BCL-10-MALT1 signalling in protective and pathological immunity. *Nat. Rev. Immunol.* **19**, 118–134 (2019).
3. I. Meininger, R. A. Griesbach, D. Hu, T. Gehring, T. Seeholzer, A. Bertossi, J. Kranich, A. Oeckinghaus, A. C. Eitelhuber, U. Greczmiel, A. Gewies, M. Schmidt-Supprian, J. Ruland, T. Brocker, V. Heissmeyer, F. Heyd, D. Krappmann, Alternative splicing of MALT1 controls signalling and activation of $CD4^+$ T cells. *Nat. Commun.* **7**, 11292 (2016).
4. H. Noels, G. van Loo, S. Hagens, V. Broeckx, R. Beyaert, P. Marynen, M. Baens, A novel TRAF6 binding site in MALT1 defines distinct mechanisms of NF-kappaB activation by API2 MALT1 fusions. *J. Biol. Chem.* **282**, 10180–10189 (2007).
5. L. Sun, L. Deng, C. K. Ea, Z. P. Xia, Z. J. Chen, The TRAF6 ubiquitin ligase and TAK1 kinase mediate IKK activation by BCL10 and MALT1 in T lymphocytes. *Mol. Cell* **14**, 289–301 (2004).
6. T. J. O'Neill, T. Seeholzer, A. Gewies, T. Gehring, F. Giesert, I. Hamp, C. Graß, H. Schmidt, K. Kriegsmann, M. J. Tofaute, K. Demski, T. Poth, M. Rosenbaum, T. Schnalzger, J. Ruland, M. Göttlicher, M. Kriegsmann, R. Naumann, V. Heissmeyer, O. Plettenburg, W. Wurst, D. Krappmann, TRAF6 prevents fatal inflammation by homeostatic suppression of MALT1 protease. *Sci. Immunol.* **6**, eabh2095 (2021).
7. P. A. Bell, S. Scheuermann, F. Renner, C. L. Pan, H. Y. Lu, S. E. Turvey, F. Bornancin, C. H. Régnier, C. M. Overall, Integrating knowledge of protein sequence with protein function for the prediction and validation of new MALT1 substrates. *Comput. Struct. Biotechnol. J.* **20**, 4717–4732 (2022).
8. B. N. Moud, F. Ober, T. J. O'Neill, D. Krappmann, MALT1 substrate cleavage: What is it good for? *Front. Immunol.* **15**, 1412347 (2024).
9. A. Demeyer, E. Van Nuffel, G. Baudelet, Y. Driege, M. Kreike, D. Muyllaert, J. Staal, R. Beyaert, MALT1-deficient mice develop atopic-like dermatitis upon aging. *Front. Immunol.* **10**, 2330 (2019).
10. A. A. Ruefli-Brasse, D. M. French, V. M. Dixit, Regulation of NF-kappaB-dependent lymphocyte activation and development by paracaspase. *Science* **302**, 1581–1584 (2003).
11. J. Ruland, G. S. Duncan, A. Wakeham, T. W. Mak, Differential requirement for Malt1 in T and B cell antigen receptor signaling. *Immunity* **19**, 749–758 (2003).
12. F. Bornancin, F. Renner, R. Touil, H. Sic, Y. Kolb, I. Touil-Allaoui, J. S. Rush, P. A. Smith, M. Bigaud, U. Junker-Walker, C. Burkhart, J. Dawson, S. Niwa, A. Katopodis, B. Nuesslein-Hildesheim, G. Weckbecker, G. Zenke, B. Kinzel, E. Traggiai, D. Brenner, A. Brüstle, M. St Paul, N. Zamurovic, K. D. McCoy, A. Rolink, C. H. Régnier, T. W. Mak, P. S. Ohashi, D. D. Patel, T. Calzascia, Deficiency of MALT1 paracaspase activity results in unbalanced regulatory and effector T and B cell responses leading to multiorgan inflammation. *J. Immunol.* **194**, 3723–3734 (2015).
13. A. Gewies, O. Gorka, H. Bergmann, K. Pechloff, F. Petermann, K. M. Jeltsch, M. Rudelius, M. Kriegsmann, W. Weichert, M. Horsch, J. Beckers, W. Wurst, M. Heikenwalder, T. Korn, V. Heissmeyer, J. Ruland, Uncoupling Malt1 threshold function from paracaspase activity results in destructive autoimmune inflammation. *Cell Rep.* **9**, 1292–1305 (2014).
14. M. Jaworski, B. J. Marsland, J. Gehrig, W. Held, S. Favre, S. A. Luther, M. Perroud, D. Golshayan, O. Gaide, M. Thome, Malt1 protease inactivation efficiently dampens immune responses but causes spontaneous autoimmunity. *EMBO J.* **33**, 2765–2781 (2014).
15. M. Rosenbaum, A. Gewies, K. Pechloff, C. Heuser, T. Engleitner, T. Gehring, L. Hartjes, S. Krebs, D. Krappmann, M. Kriegsmann, W. Weichert, R. Rad, C. Kurts, J. Ruland, Bcl10-controlled Malt1 paracaspase activity is key for the immune suppressive function of regulatory T cells. *Nat. Commun.* **10**, 2352 (2019).
16. N. Kutukculer, T. Seeholzer, T. J. O'Neill, C. Graß, A. Aykut, N. E. Karaca, A. Durmaz, O. Cogulu, G. Aksu, T. Gehring, A. Gewies, D. Krappmann, Human immune disorder associated with homozygous hypomorphic mutation affecting MALT1B splice variant. *J. Allergy Clin. Immunol.* **147**, 775–778.e8 (2021).
17. S. Chen, L. C. Francioli, J. K. Goodrich, R. L. Collins, M. Kanai, Q. Wang, J. Alföldi, N. A. Watts, C. Vittal, L. D. Gauthier, T. Poterba, M. W. Wilson, Y. Tarasova, W. Phu, R. Grant, M. T. Yohannes, Z. Koenig, Y. Farjoun, E. Banks, S. Donnelly, S. Gabriel, N. Gupta, S. Ferriera, C. Tolonen, S. Novod, L. Bergelson, D. Roazen, V. Ruano-Rubio, M. Covarrubias, C. Llanwarne, N. Petrillo, G. Wade, T. Jeandet, R. Munshi, K. Tibbetts, A. O'Donnell-Luria, M. Solomonson, C. Seed, A. R. Martin, M. E. Talkowski, H. L. Rehm, M. J. Daly, G. Tiao, B. M. Neale, D. G. MacArthur, K. J. Karczewski, A genomic mutational constraint map using variation in 76,156 human genomes. *Nature* **625**, 92–100 (2024).
18. L. Chen, J. Wang, J. Liu, H. Wang, C. D. Hillyer, L. Blanc, X. An, N. Mohandas, Dynamic changes in murine erythropoiesis from birth to adulthood: Implications for the study of murine models of anemia. *Blood Adv.* **5**, 16–25 (2020).
19. K. M. Jeltsch, D. Hu, S. Brenner, J. Zöller, G. A. Heinz, D. Nagel, K. U. Vogel, N. Rehage, S. C. Warth, S. L. Edelmann, R. Gloury, N. Martin, C. Lohs, M. Lech, J. E. Stehklein, A. Geerlof, E. Kremmer, A. Weber, H. J. Anders, I. Schmitz, M. Schmidt-Supprian, M. Fu, H. Holtmann, D. Krappmann, J. Ruland, A. Kallies, M. Heikenwalder, V. Heissmeyer, Cleavage of roquin and regnase-1 by the paracaspase MALT1 releases their cooperatively repressed targets to promote T(H)17 differentiation. *Nat. Immunol.* **15**, 1079–1089 (2014).
20. T. Uehata, H. Iwasaki, A. Vandenbon, K. Matsushita, E. Hernandez-Cuellar, K. Kuniyoshi, T. Satoh, T. Mino, Y. Suzuki, D. M. Standley, T. Tsujimura, H. Rakugi, Y. Isaka, O. Takeuchi, S. Akira, Malt1-induced cleavage of regnase-1 in CD4(+) helper T cells regulates immune activation. *Cell* **153**, 1036–1049 (2013).
21. J. Tapial, K. C. H. Ha, T. Sterne-Weiler, A. Gohr, U. Braunschweig, A. Hermoso-Pulido, M. Quesnel-Vallières, J. Permanyer, R. Sodaei, Y. Marquez, L. Cozzuto, X. Wang, M. Gómez-Velázquez, T. Rayon, M. Manzanares, J. Ponomarenko, B. J. Blencowe, M. Irimia, An atlas of alternative splicing profiles and functional associations reveals new regulatory programs and genes that simultaneously express multiple major isoforms. *Genome Res.* **27**, 1759–1768 (2017).
22. C. Graß, F. Ober, C. Sixt, B. N. Moud, I. Antoshkina, F. Eberstadt, A. Puhach, G. Avar, A. Keßler, T. J. O'Neill, T. Seeholzer, J. Kranich, T. Brocker, K. Lammens, M. P. Menden, C. E. Zielinski, D. Krappmann, LUBAC modulates CBM complex functions downstream of TRAF6 in T cells. *Nat. Commun.* **16**, 9899 (2025).
23. T. J. O'Neill, A. Gewies, T. Seeholzer, D. Krappmann, TRAF6 controls T cell homeostasis by maintaining the equilibrium of MALT1 scaffolding and protease functions. *Front. Immunol.* **14**, 1111398 (2023).
24. H. Schmidt, T. Raj, T. J. O'Neill, A. Muschaweckh, F. Giesert, A. Negraschus, K. P. Hoefig, G. Behrens, L. Esser, C. Baumann, R. Feederle, C. Plaza-Sirvent, A. Geerlof, A. Gewies, S. E. Isay, J. Ruland, I. Schmitz, W. Wurst, T. Korn, D. Krappmann, V. Heissmeyer, Unrestrained cleavage of Roquin-1 by MALT1 induces spontaneous T cell activation and the development of autoimmunity. *Proc. Natl. Acad. Sci. U.S.A.* **120**, e2309205120 (2023).
25. F. Schlauderer, T. Seeholzer, A. Desfosses, T. Gehring, M. Strauss, K. P. Hopfner, I. Gutsche, D. Krappmann, K. Lammens, Molecular architecture and regulation of BCL10-MALT1 filaments. *Nat. Commun.* **9**, 4041 (2018).
26. L. David, Y. Li, J. Ma, E. Garner, X. Zhang, H. Wu, Assembly mechanism of the CARMA1-BCL10-MALT1-TRAF6 signalosome. *Proc. Natl. Acad. Sci. U.S.A.* **115**, 1499–1504 (2018).
27. Q. Qiao, C. Yang, C. Zheng, L. Fontan, L. David, X. Yu, C. Bracken, M. Rosen, A. Melnick, E. H. Egelman, H. Wu, Structural architecture of the CARMA1/Bcl10/MALT1 signalosome: Nucleation-induced filamentous assembly. *Mol. Cell* **51**, 766–779 (2013).
28. A. N. Jones, C. Graß, I. Meininger, A. Geerlof, M. Klostermann, K. Zarnack, D. Krappmann, M. Sattler, Modulation of pre-mRNA structure by hnRNP proteins regulates alternative splicing of MALT1. *Sci. Adv.* **8**, eabp9153 (2022).
29. L. Antonioli, C. Blandizzi, P. Pacher, M. Guilliams, G. Hasko, Rethinking communication in the immune system: The quorum sensing concept. *Trends Immunol.* **40**, 88–97 (2019).
30. A. R. Almeida, I. F. Amado, J. Reynolds, J. Berges, G. Lythe, C. Molina-Paris, A. A. Freitas, Quorum-sensing in $CD4^+$ T cell homeostasis: A hypothesis and a model. *Front. Immunol.* **3**, 125 (2012).
31. A. P. Sefer, H. Abolhassani, F. Ober, B. Kayaoglu, S. Bilgic Eltan, A. Kara, B. Erman, N. Surucu Yilmaz, C. Aydogmus, S. Aydemir, L. M. Charbonnier, B. Kolukisa, G. Azizi, S. Delavari, T. Momen, S. Aliyeva, Y. Kendir Demirkol, S. Tekin, A. Kiykim, O. F. Baser, H. Cokugras, M. Gursel, E. Karakoc-Aydiner, A. Ozen, D. Krappmann, T. A. Chatila, N. Rezaei, S. Baris, Expanding the clinical and immunological phenotypes and natural history of MALT1 deficiency. *J. Clin. Immunol.* **42**, 634–652 (2022).
32. M. Sonoda, M. Ishimura, K. Eguchi, Y. Yada, N. Lenhartová, A. Shiraishi, T. Tanaka, Y. Sakai, S. Ohga, Progressive B cell depletion in human MALT1 deficiency. *Clin. Exp. Immunol.* **206**, 237–247 (2021).
33. H. Y. Lu, C. M. Biggs, G. Blanchard-Rohner, S. Y. Fung, M. Sharma, S. E. Turvey, Germline CBM-opathies: From immunodeficiency to atopy. *J. Allergy Clin. Immunol.* **143**, 1661–1673 (2019).
34. M. Brvar, T. J. O'Neill, O. Plettenburg, D. Krappmann, An updated patent review of MALT1 inhibitors (2021-present). *Expert Opin. Ther. Pat.* **35**, 639–656 (2025).
35. B. Namjou, C. B. Choi, I. T. Harley, M. E. Alarcon-Riquelme, J. A. Kelly, S. B. Glenn, J. O. Ojwang, A. Adler, K. Kim, C. J. Gallant, S. A. Boackle, L. A. Criswell, R. P. Kimberly, E. E. Brown, J. Edberg, G. S. Alarcon, A. M. Stevens, C. O. Jacob, G. S. Gilkeson, D. L. Kamen, B. P. Tsao, J. M. Anaya, E. M. Kim, S. Y. Park, Y. K. Sung, J. M. Guthridge, J. T. Merrill, M. Petri, R. Ramsey-Goldman, L. M. Vila, T. B. Niewold, J. Martin, B. A. Pons-Estel, T. J. Vyse, B. I. Freedman, K. L. Moser, P. M. Gaffney, A. H. Williams, M. E. Comeau, J. D. Reveille, C. Kang, J. A. James, R. H. Scofield, C. D. Langefeld, K. M. Kaufman, J. B. Harley, S. C. Bae, Evaluation of TRAF6 in a large multiancestral lupus cohort. *Arthritis Rheum.* **64**, 1960–1969 (2012).
36. S. Raychaudhuri, B. P. Thomson, E. F. Remmers, S. Eyre, A. Hinks, C. Guiducci, J. J. Catanese, G. Xie, E. A. Stahl, R. Chen, L. Alfredsson, C. I. Amos, K. G. Ardlie, A. Barton, J. Bowes, N. P. Burtt, M. Chang, J. Coblyn, K. H. Costenbader, L. A. Criswell, J. B. Crusius, J. Cui,

P. L. De Jager, B. Ding, P. Emery, E. Flynn, P. Harrison, L. J. Hocking, T. W. Huizinga, D. L. Kastner, X. Ke, F. A. Kurreeman, A. T. Lee, X. Liu, Y. Li, P. Martin, A. W. Morgan, L. Padyukov, D. M. Reid, M. Seielstad, M. F. Seldin, N. A. Shadick, S. Steer, P. P. Tak, W. Thomson, A. H. van der Helm-van Mil, I. E. van der Horst-Bruinsma, M. E. Weinblatt, A. G. Wilson, G. J. Wolbink, P. Wordsworth, D. Altshuler, E. W. Karlson, R. E. Toes, N. de Vries, A. B. Begovich, K. A. Siminovitch, J. Worthington, L. Klareskog, P. K. Gregersen, M. J. Daly, R. M. Plenge, Genetic variants at CD28, PRDM1 and CD2/CD58 are associated with rheumatoid arthritis risk. *Nat. Genet.* **41**, 1313–1318 (2009).

37. K. Martin, U. Junker, E. Tritto, E. Sutter, T. Rubic-Schneider, H. Morgan, S. Niwa, J. Li, A. Schlapbach, D. Walker, M. Bigaud, C. Beerli, A. Littlewood-Evans, B. Rudolph, M. Laisney, D. Ledieu, K. Beltz, J. Quancard, F. Bornancin, N. Zamurovic Ribrioux, T. Calzascia, Pharmacological Inhibition of MALT1 protease leads to a progressive IPEX-like pathology. *Front. Immunol.* **11**, 745 (2020).
38. T. J. O'Neill, D. Krappmann, A. Gewies, Optimized CRISPR-Cas9-based strategy for complex gene targeting in murine embryonic stem cells for germline transmission. *Bio Protoc* **12**, e4423 (2022).
39. W. T. Poueymirou, W. Auerbach, D. Frendewey, J. F. Hickey, J. M. Escaravage, L. Esau, A. T. Dore, S. Stevens, N. C. Adams, M. G. Dominguez, N. W. Gale, G. D. Yancopoulos, T. M. DeChiara, D. M. Valenzuela, F0 generation mice fully derived from gene-targeted embryonic stem cells allowing immediate phenotypic analyses. *Nat. Biotechnol.* **25**, 91–99 (2007).
40. S. E. Troder, L. K. Ebert, L. Butt, S. Assenmacher, B. Schermer, B. Zevnik, An optimized electroporation approach for efficient CRISPR/Cas9 genome editing in murine zygotes. *PLoS One* **13**, e0196891 (2018).
41. G. Köhler, C. Milstein, Continuous cultures of fused cells secreting antibody of predefined specificity. *Nature* **256**, 495–497 (1975).

Acknowledgments: We thank S. Dhawan, K. Demski, and K. Herdt for excellent technical support for binding studies, genotyping, and qPCR. We thank F. Giehler and A. Kieser for help with AlphaScreen. IκBNS antibody was kindly provided by V. Heissmeyer. We thank M. Schmidt-Supprian for helpful discussion. **Funding:** This work was supported by Deutsche Forschungsgemeinschaft (DFG) SFB 1054 (ID 210592381) projects A04 Deutsche Krebshilfe (project 70115440) to D.K. **Author contributions:** Conceptualization: T.J.O., C.G., A.G., J.S., and D.K. Methodology: T.J.O., C.G., A.G., L.-M.H., R.F., J.S., R.B., F.G., W.W., R.N., and D.K. Resources: A.F., R.F., F.G., L.-M.H., W.W., and N.K. Investigation: T.J.O., C.G., A.G., S.C., T.G., T.S., and L.-M.H. Validation: T.J.O., C.G., A.G., L.-M.H., F.G., and D.K. Formal analysis: T.J.O., C.G., A.G., and L.-M.H. Visualization: T.J.O., C.G., A.G., and D.K. Funding acquisition: W.W., D.K., and R.B. Project administration: T.J.O., C.G., A.G., W.W., and D.K. Supervision: T.J.O., A.G., R.B., W.W., and D.K. Writing—original draft: T.J.O., C.G., A.G., and D.K. Writing—review and editing: T.J.O., C.G., A.G., T.S., L.-M.H., R.F., J.S., R.B., W.W., N.K., and D.K. **Competing interests:** The authors declare that they have no competing interests. **Data, code, and materials availability:** All data needed to evaluate and reproduce the results in the paper are present in the paper and/or the Supplementary Materials. No new codes have been generated for this work. Materials are available upon reasonable request. The transgenic mice *Malt1* ED, *Malt1* A/A, and *Malt1* B/B can be provided by D.K. pending scientific review and a completed material transfer agreement with Helmholtz Munich. Requests for materials and transgenic mice should be submitted to D.K. (daniel.krappmann@helmholtz-munich.de).

Submitted 17 March 2026
Accepted 8 July 2026
Published 12 August 2026
10.1126/sciadv.aeh2835

ScienceAdvances

MALT1 alternative splicing—A molecular rheostat for balancing immune activation and homeostasis

Thomas J. O'Neill, Carina Graß, Andreas Gewies, Sofia Coelho, Torben Gehring, Thomas Seeholzer, Lesca-Miriam Holdt, Andrew Flatley, Regina Feederle, Jens Staal, Rudi Beyaert, Florian Giesert, Wolfgang Wurst, Necil Kutukculer, Ronald Naumann, and Daniel Krappmann

Sci. Adv. **12** (33), eaeh2835. DOI: 10.1126/sciadv.aeh2835

Science Advances (ISSN 2375-2548) is published by the American Association for the Advancement of Science. 1200 New York Avenue NW, Washington, DC 20005. The title *Science Advances* is a registered trademark of AAAS.